

NO-A165 274

OBSERVATION OF MECHANISM FOR HIGHER OPERATING
TEMPERATURE EXTRINSIC DETECTORS(U) AIR FORCE WRIGHT
AERONAUTICAL LABS WRIGHT-PATTERSON AFB OH
G J BROWN ET AL. MAY 85 AFMIL-TR-85-4012 F/G 17/

141

UNCLASSIFIED

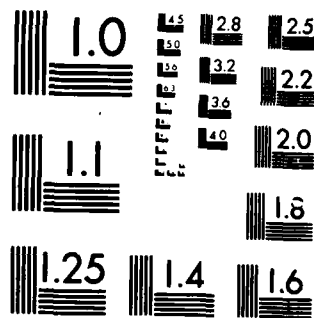
F/G 17/8

NL⁺

END

FIVE MINUTE

DTC



MICROCOPY RESOLUTION TEST CHART
NATIONAL BUREAU OF STANDARDS-1963-A

2

AD-A165 274



OBSERVATION OF MECHANISM FOR HIGHER OPERATING TEMPERATURE EXTRINSIC DETECTORS

Gail J. Brown
Melvin C. Ohmer
David Fischer

Laser & Optical Materials Branch
Electromagnetic Materials Division

Steve Smith
Frank Szmulowicz
University of Dayton
Research Institute

Shaun McGuigan
Universal Energy Systems

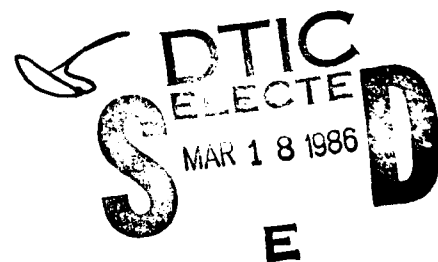
May 1985

Interim Report for Period March 1981 - August 1983

Approved for public release, distribution unlimited.

DTIC FILE COPY

MATERIALS LABORATORY
AIR FORCE WRIGHT AERONAUTICAL LABORATORIES
AIR FORCE SYSTEMS COMMAND
WRIGHT-PATTERSON AIR FORCE BASE, OHIO 45433




86 3-17 220

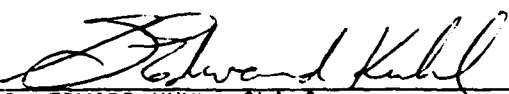
NOTICE

When Government drawings, specifications, or other data are used for any purpose other than in connection with a definitely related Government procurement operation, the United States Government thereby incurs no responsibility nor any obligation whatsoever; and the fact that the government may have formulated, furnished, or in any way supplied the said drawings, specifications, or other data, is not to be regarded by implication or otherwise as in any manner licensing the holder or any other person or corporation, or conveying any rights or permission to manufacture use, or sell any patented invention that may in any way be related thereto.


This report has been reviewed by the Office of Public Affairs (ASD/PA) and is releasable to the National Technical Information Service (NTIS). At NTIS, it will be available to the general public, including foreign nations.

This technical report has been reviewed and is approved for publication.


GAIL J. BROWN
Project Monitor
Laser & Optical Materials Branch


G. EDWARD KUHL, Chief
Laser & Optical Materials Branch
Electromagnetic Materials Division

FOR THE COMMANDER


MERRILL L. MINGES, Chief
Electromagnetic Materials Division
Materials Laboratory

"If your address has changed, if you wish to be removed from our mailing list, or if the addressee is no longer employed by your organization please notify AFWAL/MLPO W-PAFB, OH 45433 to help us maintain a current mailing list".

Copies of this report should not be returned unless return is required by security considerations, contractual obligations, or notice on a specific document.

Unclassified

SECURITY CLASSIFICATION OF THIS PAGE

REPORT DOCUMENTATION PAGE

1a. REPORT SECURITY CLASSIFICATION UNCLASSIFIED			1b. RESTRICTIVE MARKINGS		
2a. SECURITY CLASSIFICATION AUTHORITY			3. DISTRIBUTION/AVAILABILITY OF REPORT		
2b. DECLASSIFICATION/DOWNGRADING SCHEDULE			Approved for public release; distribution unlimited.		
4. PERFORMING ORGANIZATION REPORT NUMBER(S)			5. MONITORING ORGANIZATION REPORT NUMBER(S) AFWAL-TR-85-4012		
6a. NAME OF PERFORMING ORGANIZATION Materials Laboratory (AFWAL/MLPO) Air Force Wright Aeronautical Laboratories AFSC		6b. OFFICE SYMBOL (If applicable) AFWAL/MLPO		7a. NAME OF MONITORING ORGANIZATION	
6c. ADDRESS (City, State and ZIP Code) AFWAL/MLPO Wright-Patterson AFB, OH 45433-6533			7b. ADDRESS (City, State and ZIP Code)		
8a. NAME OF FUNDING/SPONSORING ORGANIZATION		8b. OFFICE SYMBOL (If applicable)		9. PROCUREMENT INSTRUMENT IDENTIFICATION NUMBER	
8c. ADDRESS (City, State and ZIP Code)			10. SOURCE OF FUNDING NOS.		
			PROGRAM ELEMENT NO.	PROJECT NO.	TASK NO.
			61102F	2306	2306Q
11. TITLE (Include Security Classification) Observation of Mechan- ism for Higher Operating Temperature Extrinsic			WORK UNIT NO. 2306Q106		
12. PERSONAL AUTHOR(S) Gail J. Brown, Melvin C. Ohmer & David Fischer, AFWAL/MLPO, Steve Smith & Frank Szmulowicz, University of Dayton, Shawn McGuigan, UES					
13a. TYPE OF REPORT Interim		13b. TIME COVERED FROM Mar 81 To Aug 83		14. DATE OF REPORT (Yr., Mo., Day) May 1985	
15. PAGE COUNT 56					
16. SUPPLEMENTARY NOTATION					
17. COSATI CODES			18. SUBJECT TERMS (Continue on reverse if necessary and identify by block number)		
FIELD	GROUP	SUB. GR.	Silicon, indium, electron irradiation, x-levels, photocon- ductivity, photothermal ionization, Hall effect, infrared absorption, extrinsic detectors, counterdoping		
19. ABSTRACT (Continue on reverse if necessary and identify by block number) Spectral photoconductivity, detectivity, infrared absorption and Hall effect transport measurements were used to study the electrical and optical properties of Si:In that had been irradiated with 1 MeV electrons. The Hall effect and infrared absorption measurements showed no unusual behaviour before or after irradiation. The photoconductivity and detectivity measurements showed a large improvement in the operating temperature range of the Si:In material after electron irradiation. Before irradiation, the detector signal became swamped by noise at 22K. After irradiation, the signal was maintained up to 80K. The magnitude of the photoresponse versus temperature remained constant up to 65K at which temperature detector noise began to set in. A constant D* peak value of 2.2×10^{10} (cm-Hz ^{1/2} /Watt) was measured up to 60K.					
20. DISTRIBUTION/AVAILABILITY OF ABSTRACT UNCLASSIFIED/UNLIMITED <input checked="" type="checkbox"/> SAME AS RPT. <input type="checkbox"/> DTIC USERS <input type="checkbox"/>			21. ABSTRACT SECURITY CLASSIFICATION Unclassified		
22a. NAME OF RESPONSIBLE INDIVIDUAL Gail J. Brown			22b. TELEPHONE NUMBER (Include Area Code) 54474		22c. OFFICE SYMBOL AFWAL/MLPO

DD FORM 1473, 83 APR

EDITION OF 1 JAN 73 IS OBSOLETE.

Unclassified

SECURITY CLASSIFICATION OF THIS PAGE

FOREWORD

This report describes the results of a systematic study of the electrical and optical properties of a wafer of Czochralski (CZ) grown silicon doped with indium. Samples from this wafer showed an unusual temperature dependence for the photoresponse after irradiation with 1 MeV electrons. The work was performed under two work units of Basic Research Task 2306Q1. Inhouse studies conducted by personnel of the Laser and Optical Materials Branch, Electromagnetic Materials Division, Materials Laboratory, Air Force Wright Aeronautical Laboratories, Wright-Patterson Air Force Base, Ohio 45433 under Project No. 2306, Task No. 2306Q1, Work Unit 2306Q106 provided the results of infrared absorption and photoconductivity measurements. The results of Hall effect measurements were provided by studies conducted by personnel of both the University of Dayton Research Institute, Dayton, Ohio 45469 under Contract No. F33615-81-C-5095, Work Unit 2306Q111, and Universal Energy Systems, Dayton, Ohio 45432 under Contract No. F33615-82-C-5001. This report covers work performed during the period March 1981 through August 1983. Detector performance measurements were conducted by personnel of the Infrared Devices Branch of the Naval Ocean Systems Center at San Diego.

Accession For	
NTIS GRA&I	<input checked="checked" type="checkbox"/>
DTIC TAB	<input type="checkbox"/>
Unannounced	<input type="checkbox"/>
Justification	

A-1

TABLE OF CONTENTS

SECTION	PAGE
I INTRODUCTION	1
II EXPERIMENTAL PROCEDURE	3
III RESULTS AND DISCUSSION	6
IV CONCLUSIONS AND RECOMMENDATIONS	38
APPENDIX PERFORMANCE MODELS OF A COUNTERDOPED DETECTOR	41
REFERENCES	47

LIST OF ILLUSTRATIONS

FIGURE		PAGE
1	Cutting Diagram for Wafer No. 099-272 Showing the Relative Positions of the Samples in the Wafer	3
2	Carrier Concentration Versus $1000/T$ for Czochralski (CZ) Si:In Sample 0745 As-Grown	7
3	Infrared Absorption Spectrum of As-Grown CZ Si:In Sample 1098	8
4	Carrier Concentration Versus $1000/T$ for CZ Si:In Sample 0745 after Electron Irradiation to $10^{17} \text{ e}^-/\text{cm}^2$	10
5	Comparison of Carrier Concentration Data for Samples 1093 (Electron Irradiated), 1130 (As-Grown) and 1120 (As-Grown) Plotted Versus Reciprocal Temperature	11
6	Comparison of Resistivity Data for Samples 1093 (Electron Irradiated), 1130 (As-Grown) and 1120 (As-Grown) Plotted Versus Reciprocal Temperature	12
7	Comparison of Hall Mobility Data for Samples 1093 (Electron Irradiated), 1130 (As-Grown) and 1120 (As-Grown) Versus $1000/T$	13
8	Carrier Concentration Versus $1000/T$ for Sample 0745 after a 350°C Anneal for 30 Minutes in a Flowing Argon Atmosphere	15
9	Carrier Concentration Versus $1000/T$ for Sample 0745 after a 550°C Anneal for 24 Hours	16
10	Infrared Absorption Spectrum of Sample 0208 after Electron Irradiation and Annealing at 550°C	17
11	Photoconductivity Spectrum of Sample 0747 after 550°C Anneal	19
12	Relative Temperature Dependence of Indium Continuum for Electron Irradiated and Annealed Si:In Samples	20
13	Normalized Photoresponse Versus Wavelength for Electron Irradiated Si:In Sample 0746 from 8K to 80K	22
14	Signal and Noise Levels Measured at 108 hz for Sample 0746	23
15	Noise Versus Frequency Data for Sample 0746	24
16	Comparison of D^* Versus Temperature for Sample 0746 and other Detector Grade Si:In Samples	25
17	Theoretical Model of Detectivity (D^*) Versus Temperature for a Conventionally Doped Detector and for the Doping Conditions of the NICE TM Detector	26

LIST OF ILLUSTRATIONS (Concluded)

FIGURE		PAGE
18	Detector Performance (D_{peak}^*) Versus Temperature for a Diffused Si:Zn Sample	27
19	Photoconductivity Spectrum of As-Grown Si:In Sample 1043	29
20	Relative Temperature Dependence of Indium Continuum for As-Grown, Annealed and Electron Irradiated Si:In Samples from Wafer 099-272	30
21	Comparison of the Photoionization Cross Sections of As-Grown and Electron Irradiated Si:In	31
22	Photoconductivity Spectrum of Electron Irradiated Si:In	32
23	Signal and Noise Levels Measured at 108 hz for Electron Irradiated Si:In Cubes	34
24	Noise Versus Frequency Data for Electron Irradiated Si:In Cube	35
25	Detector Performance (D_{peak}^*) for Electron Irradiated Si:In Cube	36
26	Comparison of NOSC and MLPO Measured Photoresponse of As-Grown Si:In Cube	37

LIST OF TABLES

TABLE		PAGE
1	Impurity Concentrations Determined by Hall and Absorption Measurements for As-Grown Si:In	6
2	Summary of the Hall Concentrations and Activation Energies of Impurities before and after Electron Irradiation for all Four CZ Si:In Samples	18
3	Comparison of Impurity Concentrations Determined by Infrared Absorption for Sample 0208 As-Grown and after Electron Irradiation and Annealing	18
4	Comparison of Impurity Concentrations (atoms/cm ³) Determined by Hall and Infrared Absorption Measurements	39

SECTION I

INTRODUCTION

This report is a rapid communication of the observation of an interesting phenomenon in photoconductivity (PC) measurements on a particular wafer of Czochralski grown Si:In. Originally the intent was to produce high concentrations of the indium-x level through electron irradiation and subsequent annealing of Si:In (References 1, 2). Hall measurements before and after irradiation and annealing did show an increase in the amount of In-X present in the sample as expected. However, while searching for the presence of In-X through photoconductivity measurements an interesting effect was observed in an electron irradiated sample that had not been annealed above room temperature. After three months at room temperature, the initial PC measurements, using a Fourier transform spectrophotometer, showed a very noisy interferogram for sample temperatures below 35K. From 40K to 65K the interferogram was good and data could be collected. Then at about 70K the interferogram became too noisy again for data collection. This behavior was quite unusual because the typical Si:In sample is run at temperatures below 35K in order to observe sharp indium excited state lines. Also, previous Si:In samples could not be run at temperatures above about 30K due to excessive low frequency noise causing an A/D overload in the signal processing electronics. Photoconductivity measurements were made on this sample again three months later. During this second testing the sample had good signal to noise from 9K to 82K. A year later the results of this second run were still repeatable.

Based on these PC results, it was decided to explore the usefulness of this material for higher temperature Si:In infrared detectors. To test the detector characteristics of this material, the electron irradiated PC sample was taken to Naval Ocean Systems Center (NOSC). Lum Eiseman and Craig Sayre of the Infrared Devices Branch performed the detector measurements on the 3mm x 5mm x 1mm sample. These initial detector measurements gave a peak in the D_{λ}^* at 70K. This result was encouraging so a second sample set was made with a more optimally designed detector configuration of 1mm x 1mm x 1mm for additional testing at NOSC. Detector measurements on this new electron irradiated sample set also produced a good D_{λ}^* vs. temperature curve but without the peak at 70K. An as-grown Si:In sample set from the same wafer could not be measured above 22K due to excessive noise in the detectors.

This report is a summary of all the absorption, Hall effect, photoconductivity and detector measurements that have been made on this unique Si:In wafer. It is still not clear what the mechanism is for the unusual temperature dependence of the electron irradiated samples. One of the mechanisms considered was that double donor divacancies formed during irradiation acted as a counterdopant for the shallow acceptors. This concept lead to the acronym NICETM (New Improved Counterdoped Extrinsic) to describe the electron irradiated material. It is possible that a better understanding of this NICETM material could lead to Si:In detector arrays of higher operating temperature.

SECTION II

EXPERIMENTAL PROCEDURE

1. SAMPLE PREPARATION

The starting material for this study was a two inch diameter, Czochralski grown Si:In wafer labelled No. 099-272. This wafer was first polished, cleaned and then four samples numbered 0208, 0746, 0747, and 0745 were cut from this wafer (see cutting diagram for details, Figure 1). Sample No. 0208 was cut and polished for absorption measurements. Sample 0745 was ultrasonically cut into a van der Pauw configuration (Reference 3) for Hall effect transport measurements. Samples 0746 and 0747 were cut for photoconductivity measurements. Hall and photoconductivity samples were cleaned using the standard 'RCA' two stage cleaning process (Reference 4). Ohmic contact areas were produced either using a sparking technique (Reference 5) or by pulsed laser annealing of borosilicate onto the sample surface (Reference 6). Gold wires were indium soldered directly to the contact areas.

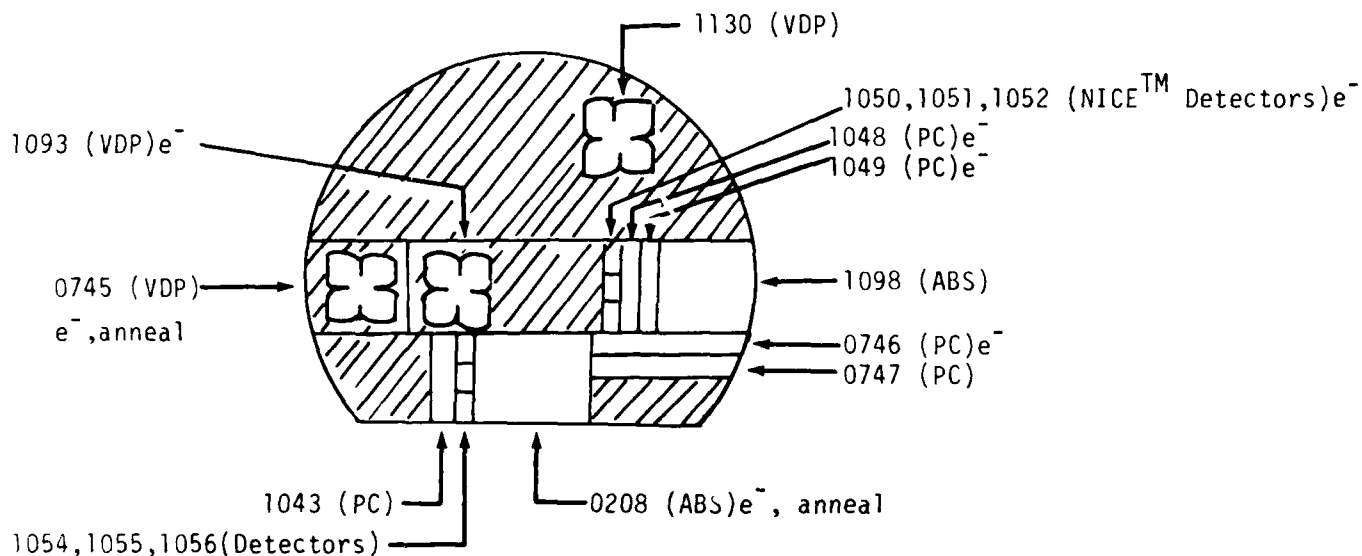


Figure 1. Cutting Diagram for Wafer No. 099-272 Showing the Relative Positions of the Samples in the Wafer

After initial Hall and absorption measurements, samples 0208, 0745, and 0746 were electron irradiated on each side with $5 \times 10^{16} \text{ e}^-/\text{cm}^2$ with an energy of 1 MeV. This room temperature irradiation was performed with a Van de Graaff accelerator at AFWAL/AADR. Since the range of 1 MeV electrons is characterized by an LSS range of 1mm and the samples were 1mm thick, the radiation profile was fairly uniform.

Later samples 0745, 0208, and 0747 were annealed at 350°C for 30 minutes in an argon ambient. And, after experimental measurements were made, these samples were again annealed at 550°C for 24 hours in an argon ambient.

A little over a year later several more samples were cut from wafer No. 099-272 (Figure 1). Also, a van der Pauw sample (1120) was cut from a second CZ Si:In wafer No. 099-290. Out of this new set of samples, samples 1093 and 1048-1052 were electron irradiated as described in the previous paragraph. The rest of the samples were left as-grown. Samples 1050-1052 and 1054-1056 were 1mm x 1mm x 1mm cubes with laser annealed contacts on two opposing cube faces. Each set of three cubes was mounted with GE 7031 varnish onto a beryllium oxide slab.

2. HALL MEASUREMENTS

Hall measurements were performed on a guarded DC Hall apparatus (Reference 7) designed for high impedance ($\sim 10^{13} \Omega$) measurements. The van der Pauw samples were mounted in a cryogenic variable temperature dewar. Experimental data was taken in the temperature range of 50K to 380K in an applied magnetic field of 1KG.

The concentrations and activation energies of impurities were obtained by a nonlinear least-squares fit to the charge balance equation:

$$P + N_D = \sum_i \frac{N_i}{1 + P(g_i/N_v) \exp(E_i/kT)} \quad (1)$$

where N_i , E_i and g_i , are the concentration, activation energy and ground state degeneracy of the i^{th} acceptor species, respectively. The donor concentration N_D is given by:

$$N_D = \sum_i N_{D_i} - \sum_k N_{A_k} \quad (2)$$

where N_{D_i} are all the donor levels and N_{A_k} are all the acceptor levels sufficiently below the Fermi level to be fully ionized over the temperature range under investigation. The density of states in the valence band, N_v , was calculated taking into account the temperature dependence of the effective hole mass and the non-parabolicity of the valence bands (References 8, 9). An empirical Hall scattering factor ($r_H \neq 1$) (Reference 10) was also used when fitting the carrier concentration data. The use of this Hall factor gives closer agreement with carrier concentrations obtained from C-V measurements, and with optically determined acceptor ionization energies in highly doped samples (Reference 11).

3. PHOTOCONDUCTIVITY MEASUREMENTS

All spectra were recorded on a Digilab model FTS-20CVX Fourier transform spectrophotometer at a resolution of 2 cm^{-1} in the infrared region from 4,000 to 200 cm^{-1} . The samples were mounted on a thin beryllium oxide slab on the cold-finger of a closed-cycle helium refrigeration system. After mounting, the samples were wired in series with a $100 \text{ k}\Omega$ load resistor, also mounted on the cold-finger. This simple circuit was biased with a DC voltage of 9V. The photoconductivity data were collected in a voltage-mode with measurements taken across the load resistor. The resulting voltage signal was fed through a pre-amplifier, adjustable gain amplifiers, and an analog to digital converter to be recorded and analyzed by computer. Data were recorded in a temperature range of 8.0K to 80K.

4. ABSORPTION MEASUREMENTS

The absorption samples were mounted on the cold-finger of a liquid helium dewar. The spectra were recorded on the same Digilab model FTS-20CVX Fourier transform spectrophotometer as the photoconductivity spectra. The absorption spectra were collected in the single beam mode at a resolution of 2 cm^{-1} in the infrared region from 4,000 to 200 cm^{-1} . The sample transmittance was referenced to an empty sample holder. A computer program was used to convert transmittance to absorption coefficient in the usual manner (Reference 12).

SECTION III

RESULTS AND DISCUSSION

Initially, Hall transport and absorption measurements were made on as-grown Si:In samples from the same wafer, numbered 0745 and 0208 respectively. Later in the study, another set of as-grown samples (1130, 1043 and 1098) were cut from this same wafer and measured by the Hall transport, photoconductivity, and absorption facilities. In addition, Hall measurements were made on a sample (1120) from another wafer of the same boule. A typical curve showing the carrier concentration fitting of the transport data for an as-grown sample (0745) from this wafer is shown in Figure 2. The as-grown material did not seem to exhibit any unusual behavior or impurity species. Similarly, the absorption measurements on the as-grown material (0208, 1098) showed nothing unusual; standard Si:In spectra were obtained. An absorption spectrum for sample 1098 is shown in Figure 3. The impurity or dopant concentrations determined by these two experiments are compared below.

TABLE 1
IMPURITY CONCENTRATIONS DETERMINED BY HALL
AND ABSORPTION MEASUREMENTS FOR AS-GROWN Si:In

Impurity or Dopant	Hall Effect (cm^{-3})		IR Absorption (cm^{-3})	
	0745	1130	0208	1098
In	2.59×10^{16}	1.52×10^{16}	3.8×10^{16}	3.6×10^{16}
In-X	--	1.92×10^{14}	--	--
B	--	--	no data	1×10^{14}
Donors	2.64×10^{14}	2.08×10^{14}	--	--
C	--	--	7×10^{16}	7×10^{16}
O	--	--	6×10^{17}	6×10^{17}

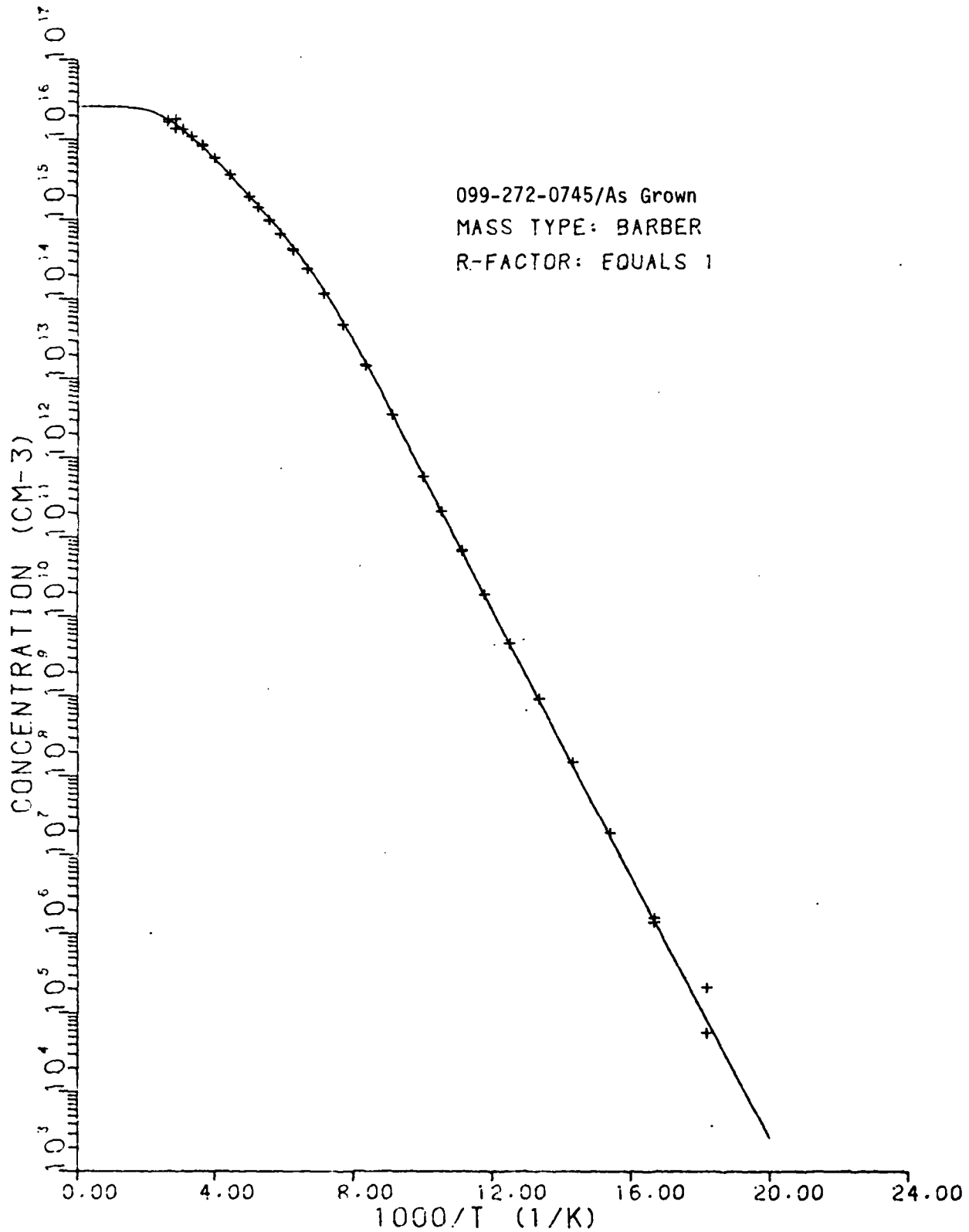


Figure 2. Carrier Concentration Versus 1000/T for Czoehralski (CZ) Si:In Sample 0745 As-Grown

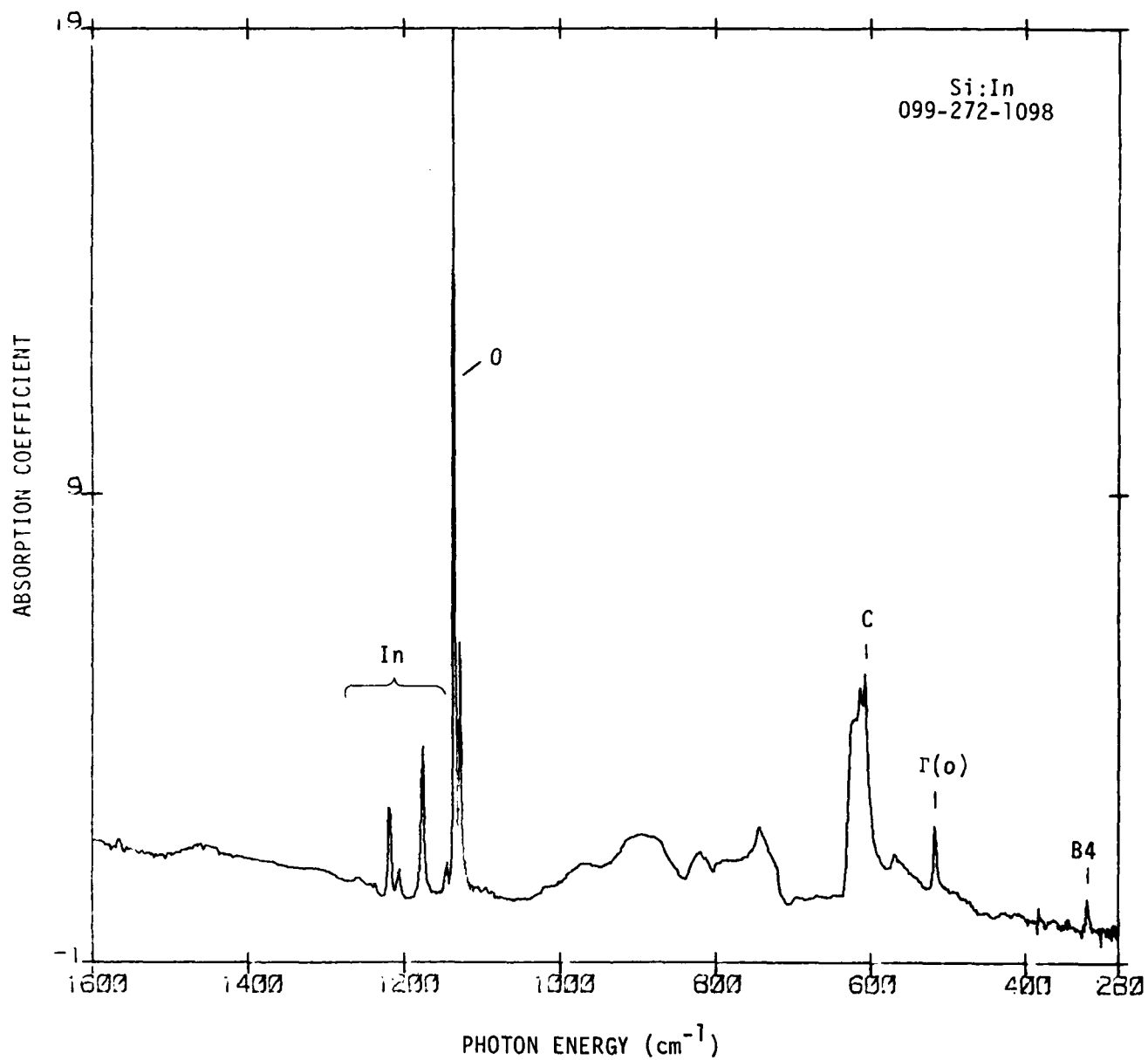


Figure 3. Infrared Absorption Spectrum of As-Grown CZ Si:In Sample 1098

The original Hall analysis of sample 0745 did not reveal the presence of indium-X and yielded an indium concentration approximately 74% higher than those found for samples 1130 and 1120. The discrepancies may be attributed to subsequent improvements in the carrier concentration fitting routines, yielding more accurate impurity concentrations and detecting shallower over-compensated impurity levels. The main improvements were the inclusion of the temperature dependent effective masses (References 8, 9) and the empirical Hall factor (Reference 10). Also, a ground state degeneracy of four is now commonly used for fitting all impurity species.

Once the as-grown material was characterized, five samples (0208 (ABS), 0745 (VDP), 1093 (VDP)¹, 0746 (PC), and 0747 (PC)) were irradiated with 1 MeV electrons. After irradiation the donor concentration of the van der Pauw samples 0745 and 1093 increased as expected (References 1, 2) by a factor of about 0.01 of the fluence (Figure 4). Similarly, if a comparison is made between the indium-X level samples 1130 and 1120, as-grown, and 1093 after electron irradiation, the concentration of this species also increased by approximately 0.01 of the electron fluence. Figures 5, 6, and 7 compare the Hall results for these three samples (1130, 1120 and 1093). The absorption (ABS) measurements showed little difference before and after irradiation. Photoconductivity (PC) measurements were made on sample 0746 approximately three months after it was electron irradiated. Normally, photo-thermal ionization spectra of doped silicon are collected in the 7K to 25K temperature range. However, no Fourier transform photoconductivity data could be collected on this sample at these low temperatures. Instead the spectrometer system showed an alarm status of an A/D overflow. This alarm can be triggered by one of three conditions: a) the AC signal is greater than ± 9.6 volts, b) there is too large of a DC offset in the signal, or c) there is an excessive amount of noise in the signal. As the sample was allowed to warm up above 30K this alarm went away and a very noisy interferogram appeared, so condition c must have triggered the alarm. Between 40K and 65K the interferogram improved and data was collected. This data showed a typical Si:In response. Afterwards the sample contacts were checked to make sure that non-ohmic contacts were not the cause of the low temperature noise. The contacts were found to be ohmic.

¹ Sample 1093 was electron irradiated at a later date.

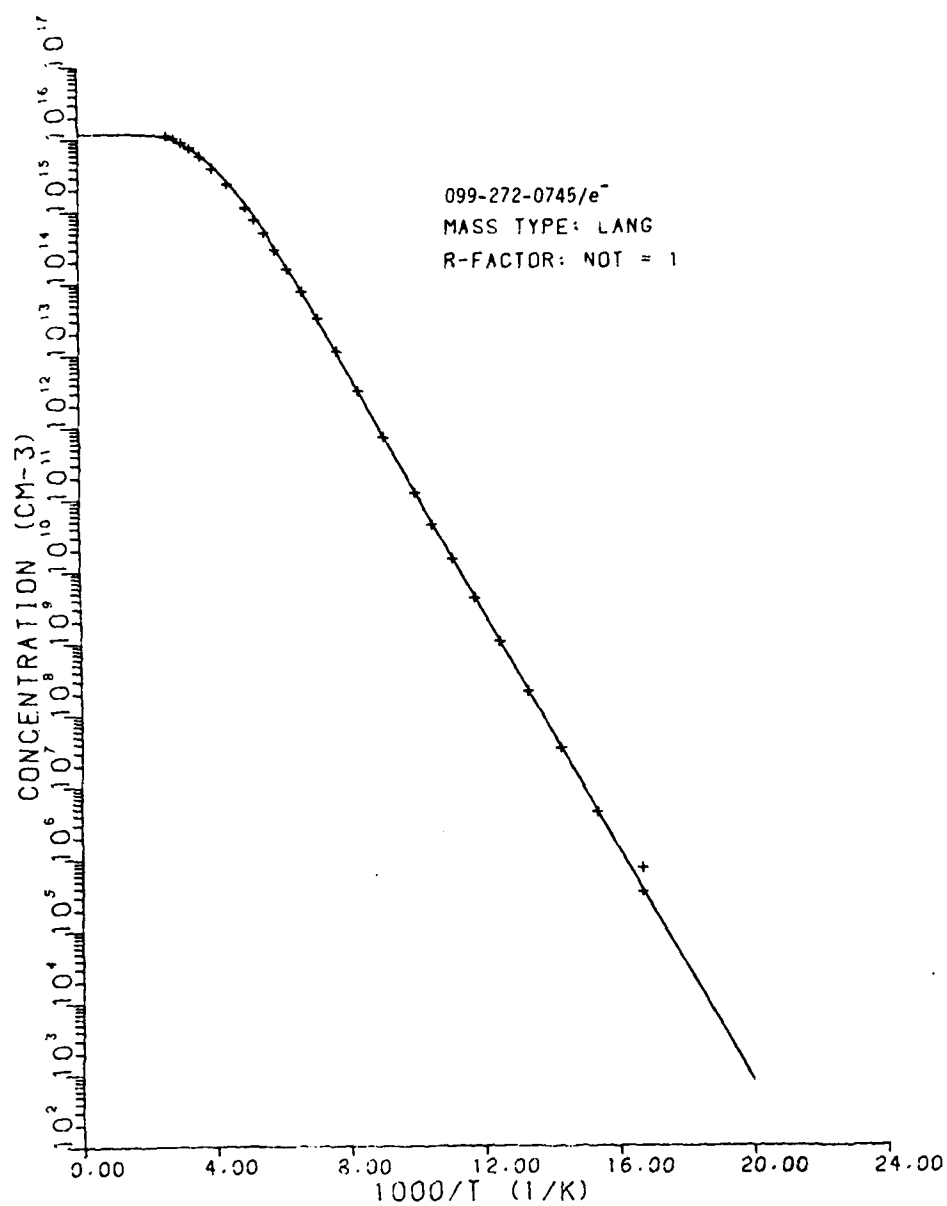


Figure 4. Carrier Concentration Versus 1000/T for CZ Si:In Sample 0745
After Electron Irradiation to 10¹⁷ e⁻/cm²

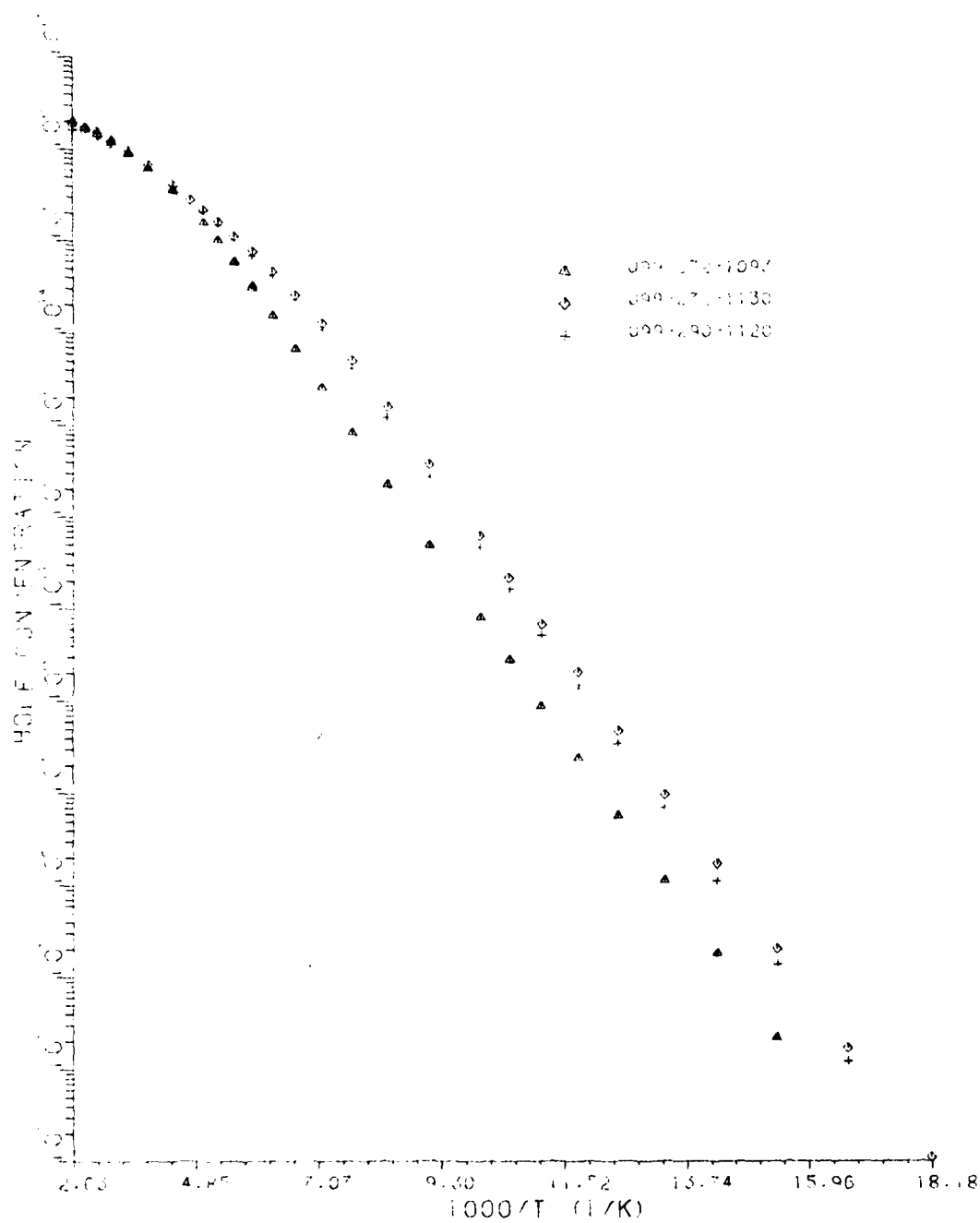


Figure 5. Comparison of Carrier Concentration Data for Samples 1093 (Electron Irradiated), 1130 (As-Grown) and 1120 (As-Grown) Plotted Versus Reciprocal Temperature

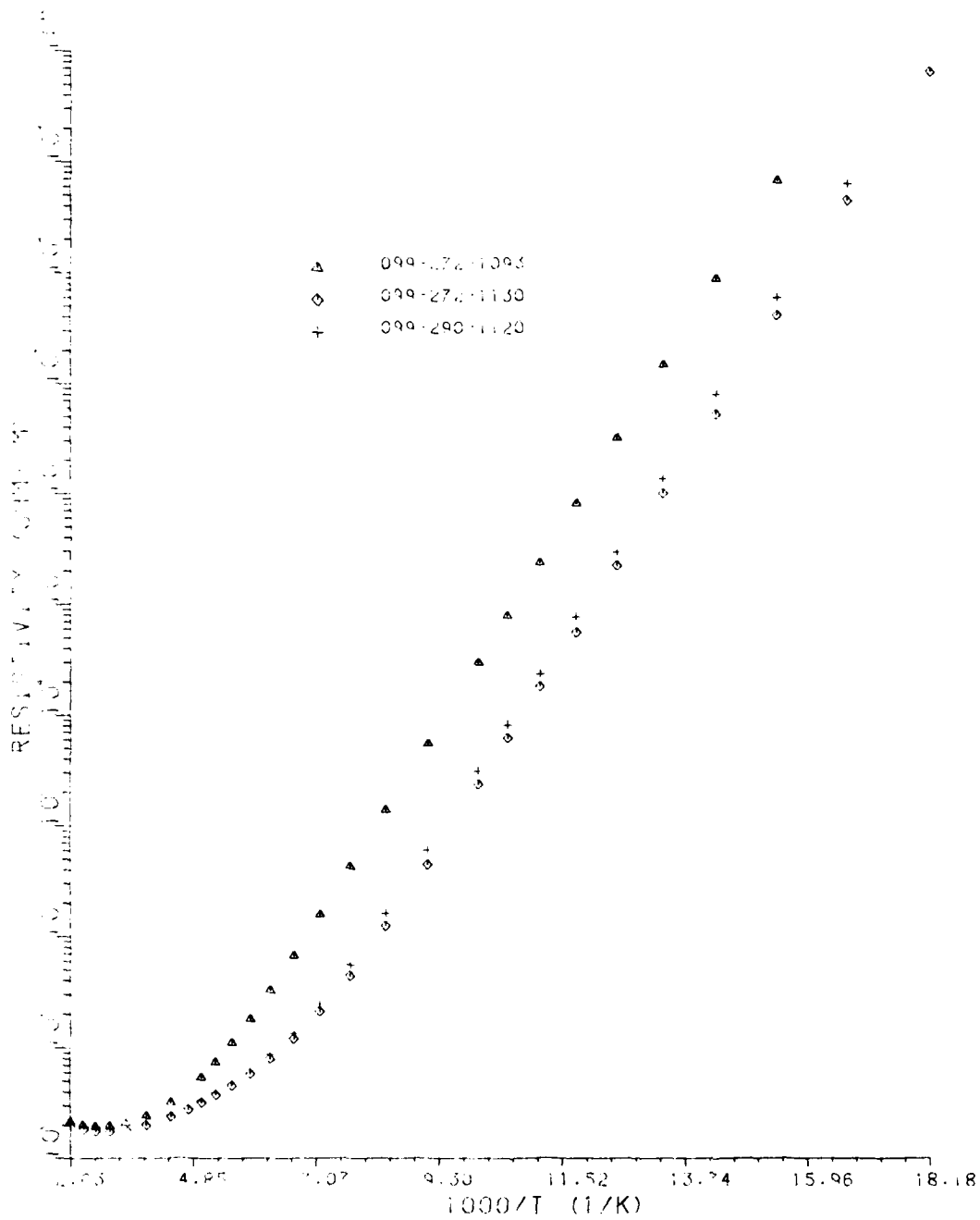


Figure 6. Comparison of Resistivity Data for Samples 1093 (Electron Irradiated), 1130 (As-Grown) and 1120 (As-Grown) Plotted Versus Reciprocal Temperature

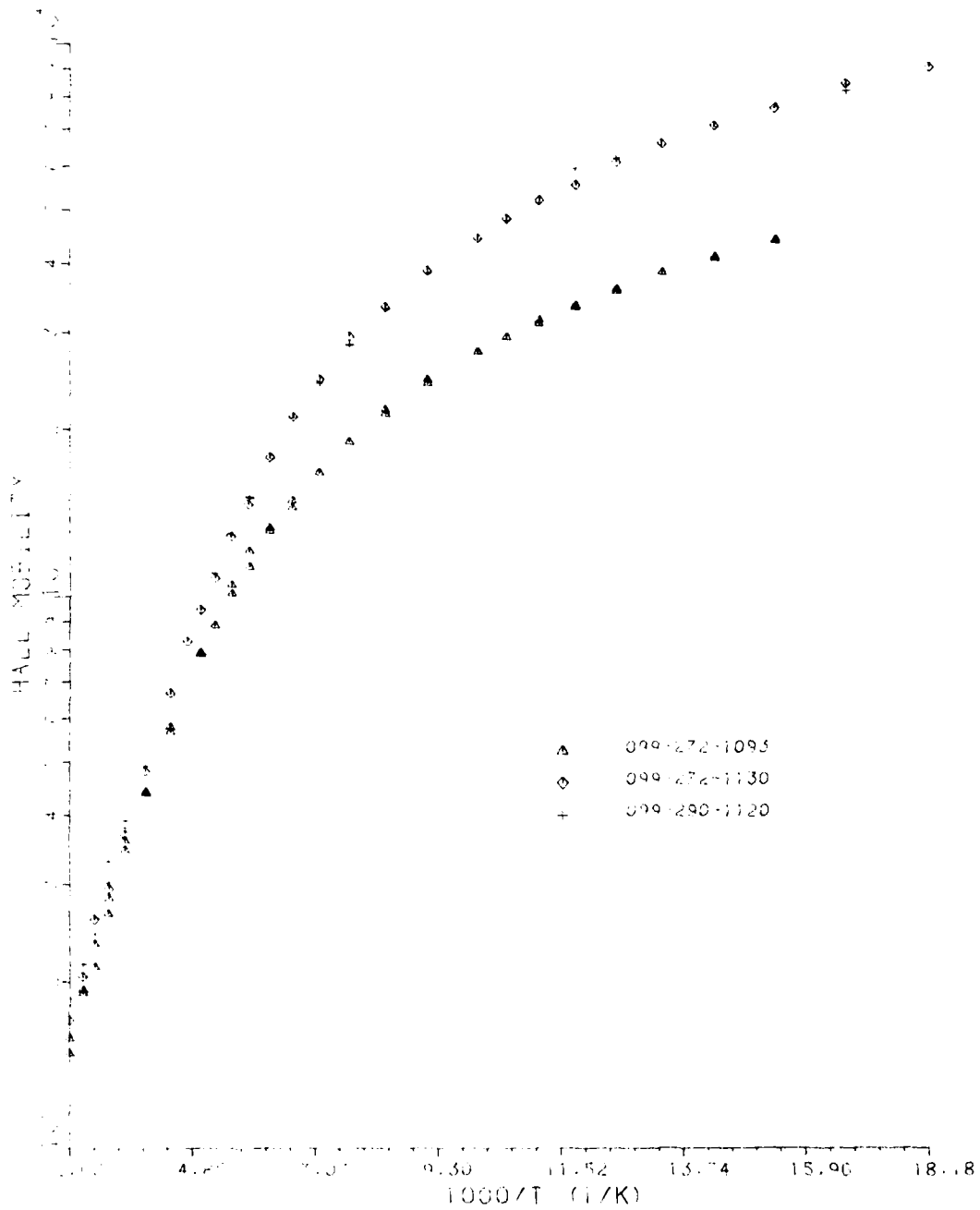


Figure 7. Comparison of Hall Mobility Data for Samples 1093 (Electron Irradiated), 1130 (As-Grown) and 1120 (As-Grown) Versus 1000/T

The next step was to anneal the electron irradiated samples at 350°C for 30 minutes to increase the In-X level. Samples 0745 (VDP), 0747 (PC), 0208 (ABS) were annealed; the electron irradiated PC sample 0746 was left at room temperature. Once Hall, PC and absorption measurements were taken, samples 0745, 0747, and 0208 were annealed at 550°C for 24 hours. Again Hall, PC, and absorption data were collected on the annealed samples. According to the Hall data, the first anneal at 350°C had little effect on either the donor or indium-X level concentrations (Figure 8). The second anneal at 550°C returned both the donor and indium-X levels back to approximately the same concentrations found in the as-grown material (Figure 9). However, the indium-X level was no longer over-compensated. These results are in good agreement with previous electron irradiation and annealing studies of Si:In (References 1, 2). The absorption data on the annealed sample (Figure 10), also showed little change when compared to the as-grown data. A summary of the Hall and absorption measurements is given in Tables 2 and 3. Before annealing, the photoconductivity spectra of sample 0747 showed only the Si:In photoionization cross section with no indium excited state lines. After the 350°C anneal, the PC spectra showed all ten indium excited state lines and an increase in the overall photoresponse. This indicates that most of the lattice damage was removed by this anneal. Also after this anneal, some boron response was present as indicated by the 2p' line of boron at 668 cm^{-1} . The boron spectrum of 0747 was even stronger after the 550°C anneal, as would be expected from the lower donor concentration after this anneal (Figure 11). And again there was an overall increase in the photoresponse of the sample with this anneal. In addition to the change in the magnitude of the photoresponse, there was also a change in the rate of increase of the indium continuum response with increasing temperature. Prior to annealing, the continuum response remained relatively flat with increasing temperature. After the 350°C anneal, the continuum response doubled in magnitude over the temperature range from 8K to 25K. Similarly, after the 550°C anneal, the magnitude of the continuum response nearly tripled over this same temperature range. The 550°C annealed sample had a rate of change of continuum response with temperature that was very similar to other unrelated as-grown Si:In samples (Figure 12). The maximum temperature the sample could be run at before a significant DC current interfered with the data collection was 27.5K. This was in agreement with several other Si:In samples from other boules and manufacturers which had previously exhibited this same behavior around 22 to 30K. This phenomenon made the unannealed electron irradiated sample 0746 seem unusual since good data with no DC offset had been collected between 40K and 65K.

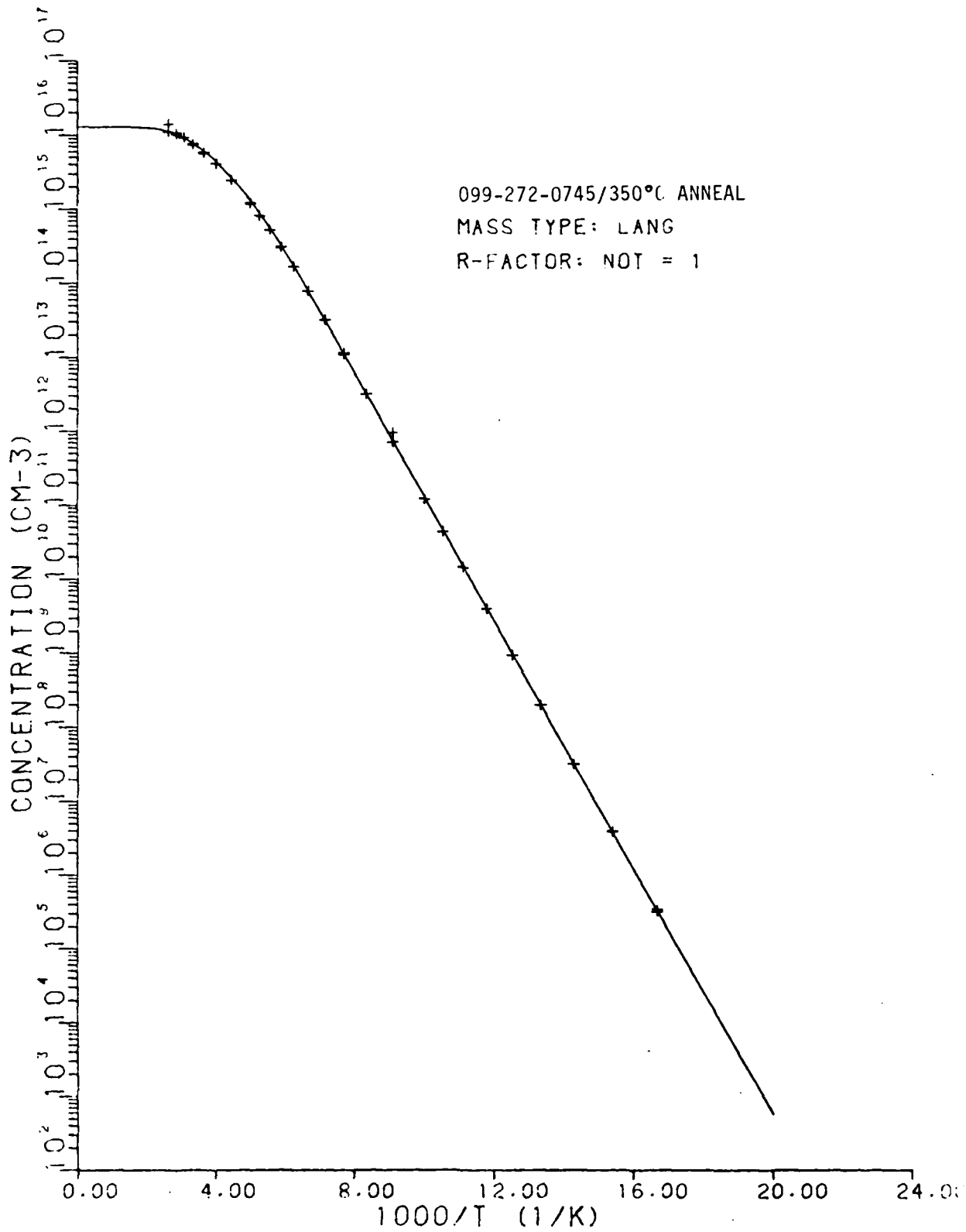


Figure 8. Carrier Concentration Versus 1000/T for Sample 0745 after a 350°C Anneal for 30 Minutes in a Flowing Argon Atmosphere

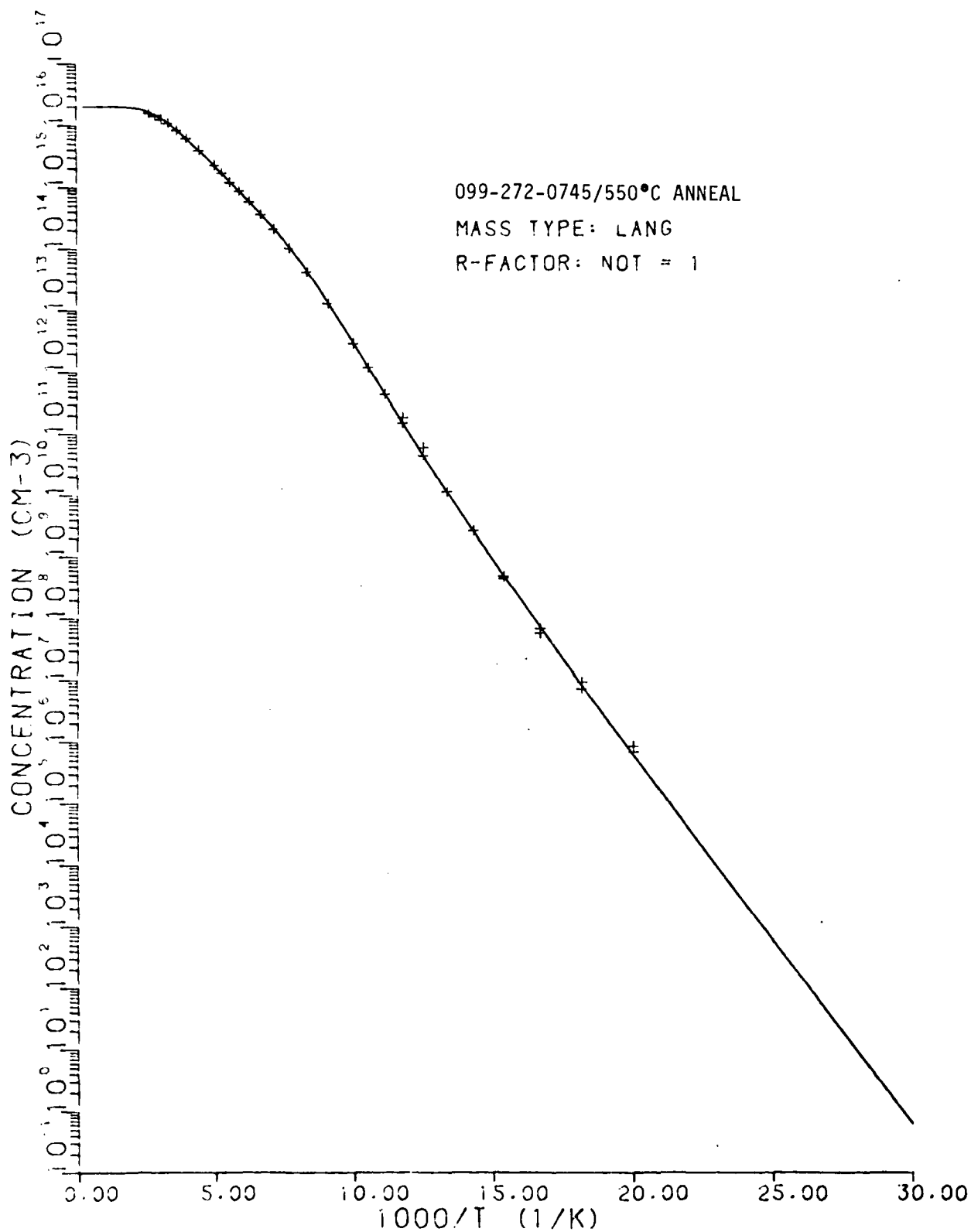


Figure 9. Carrier Concentration Versus 1000/T for Sample 0745 after a 550°C Anneal for 24 Hours

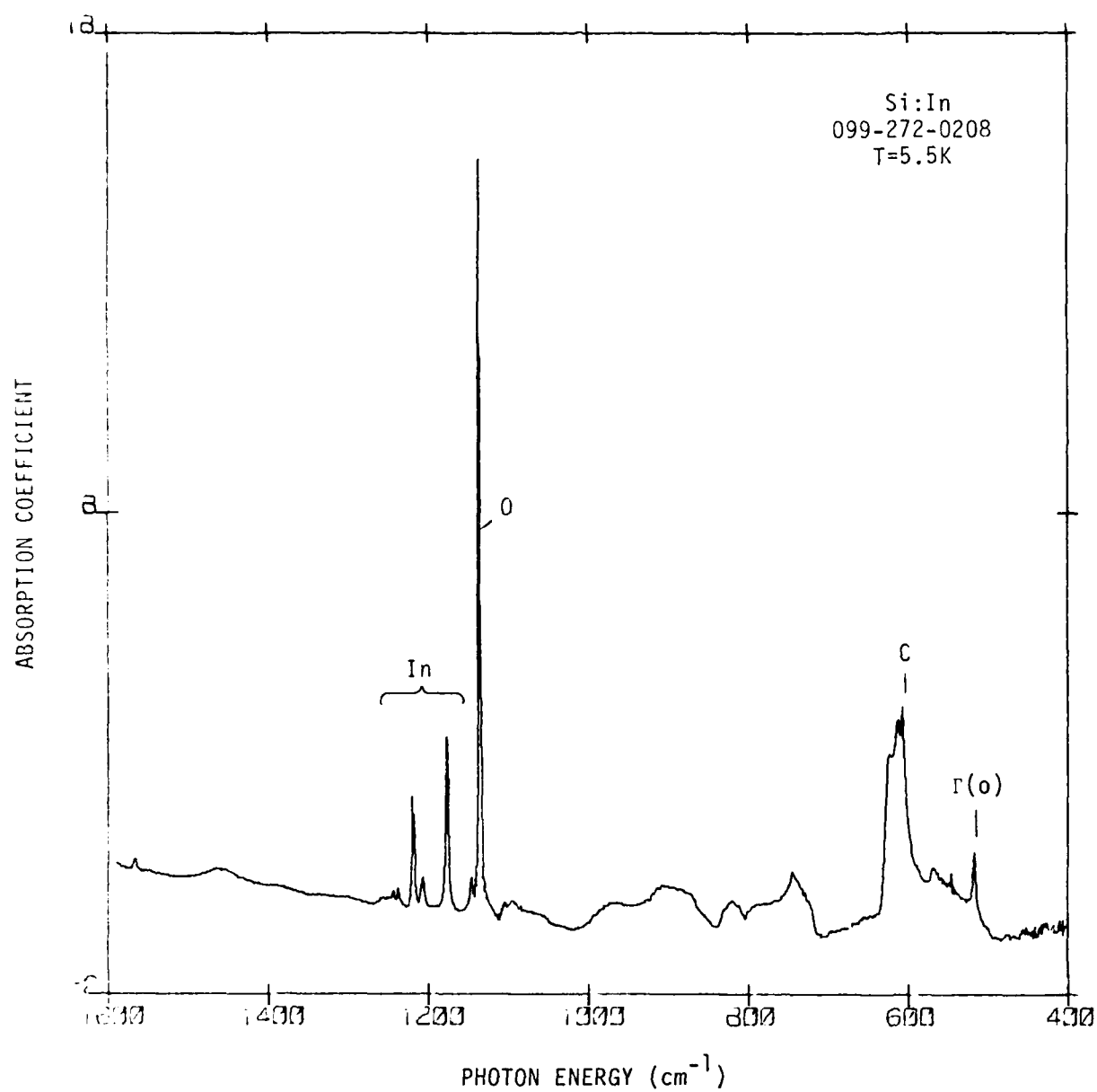


Figure 10. Infrared Absorption Spectrum of Sample 0208 after Electron Irradiation and Annealing at 550°C

TABLE 2

SUMMARY OF THE HALL CONCENTRATIONS AND ACTIVATION ENERGIES OF IMPURITIES BEFORE AND AFTER ELECTRON IRRADIATION FOR ALL FOUR CZ Si:In SAMPLES

Sample	Treatment	N_D (cm^{-3})	N_{In} (cm^{-3})	E_{In} (eV)	N_{InX} (cm^{-3})	E_{InX} (eV)
CZ Si:In ^a (1130)	As-grown	2.08×10^{14}	1.52×10^{16}	0.166	1.9×10^{14}	0.120
CZ Si:In ^a (1120)	As-grown	2.82×10^{14}	1.35×10^{16}	0.165	2.52×10^{14}	0.120
CZ Si:In ^b (0745)	As-grown	2.64×10^{14}	2.59×10^{16}	0.156	--	--
CZ Si:In ^c (0745)	After $10^{17} \text{ e}^-/\text{cm}^2$	5.64×10^{15}	1.27×10^{16}	0.152	4.57×10^{15}	0.1125
CZ Si:In ^a (1093)	After $10^{17} \text{ e}^-/\text{cm}^2$	3.37×10^{15}	1.58×10^{16}	0.165	3.12×10^{15}	0.127
CZ Si:In ^c (0745)	Annealed 30 mins/350°C	5.52×10^{15}	1.35×10^{16}	0.156	4.80×10^{15}	0.1125
CZ Si:In ^c (0745)	Annealed 24 hrs/550°C	1.77×10^{14}	1.98×10^{16}	0.157	2.23×10^{14}	0.1125

^a $g_{\text{In}}=4$, $g_{\text{InX}}=4$, Empirical $r_H \neq 1$ (Reference 10), Temperature dependent mass (References 8,9)^b $g_{\text{In}}=6$, $r_H = 1$, Barber mass^c $g_{\text{In}}=6$, $g_{\text{InX}}=2$, $r_H \neq 1$ (Reference 10), Temperature dependent mass (References 8,9)

TABLE 3

COMPARISON OF IMPURITY CONCENTRATIONS DETERMINED BY INFRARED ABSORPTION FOR SAMPLE 0208 AS-GROWN AND AFTER ELECTRON IRRADIATION AND ANNEALING

Impurity or Dopant	As-Grown	550°C
In	3.8×10^{16}	3.8×10^{16}
In-X	----	not detected
B	no data	2.8×10^{13}
C	7×10^{16}	7×10^{16}
O	6×10^{17}	6×10^{17}

Concentrations given in atoms/cm³

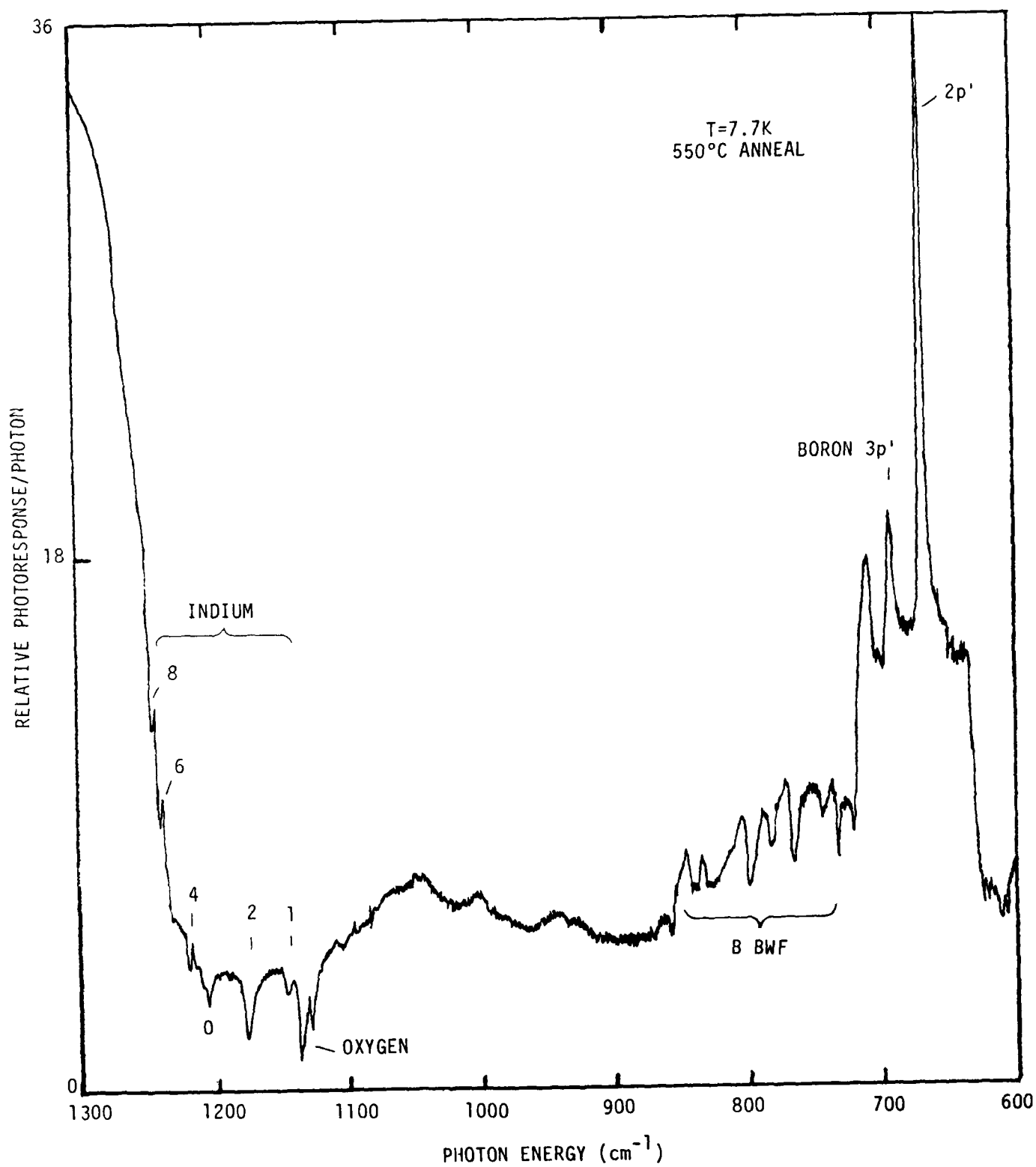


Figure 11. Photoconductivity Spectrum of Sample 0747 after 550°C Anneal

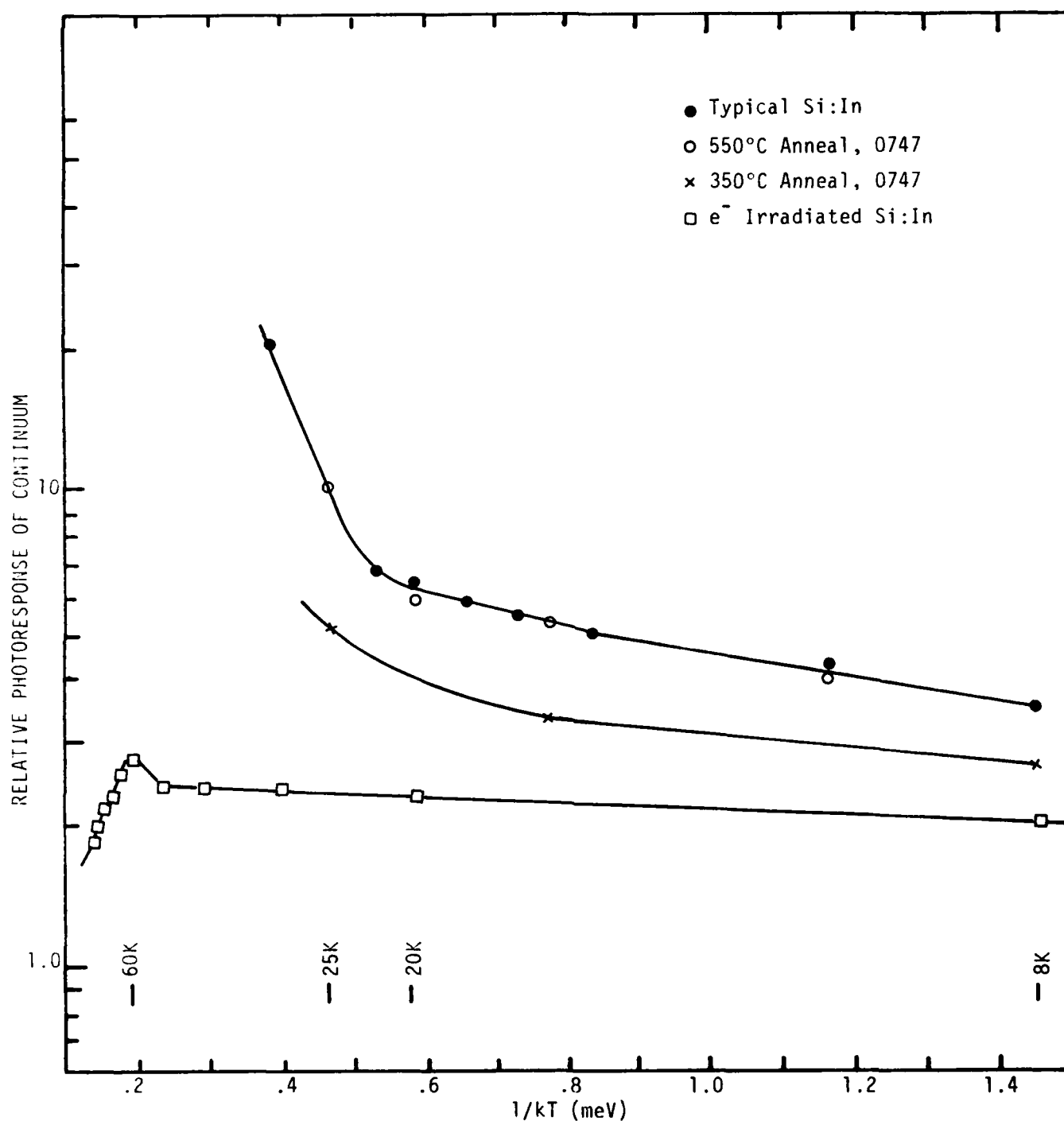


Figure 12. Relative Temperature Dependence of Indium Continuum for Electron Irradiated and Annealed Si:In Samples

Because of this unusual behavior, photoconductivity measurements on 0746 were repeated to check the temperature range over which data could be collected before a DC current appeared. After annealing for six months at room temperature, the operating range of 0746 was from 7K to 65K. After another year of room temperature annealing the operating temperature range of 0746 was from 7K to 82K. Over this temperature range there was little increase in the indium continuum response with temperature (Figure 12), and the signal to noise ratio remained fairly constant up to 60K (Figure 13).

To find out if this anomalous behavior of sample 0746 had any significance for Si:In infrared detector materials, this sample was taken to the Infrared Devices Branch of NOSC at San Diego. At NOSC, signal and noise measurements were conducted using a 500K blackbody source and a sample bias of 52 volts over a length of 0.5 cm between contacts. The resulting signal and noise levels measured at a frequency of 108hz, in a temperature range from 20K to 80K, are plotted in Figure 14. The unusual noise versus frequency data of this sample is shown in Figure 15. The noise measurements were unusual because of the decrease in the amount of noise at 70K and the humped shape of the 50K and 60K noise curves.

Using this signal and noise data at 108hz, the resulting D_{λ}^* versus temperature¹ curve is shown in Figure 16. The increase in D_{λ}^* at 70K is caused by the drop in the measured noise level at 70K. Recent theoretical modelling of counterdoped detector systems produced a graph (Figure 17) similar to this experimental data. In the model the peak at 75K is also caused by a decrease in the amount of thermal noise. This decrease results when thermally emitted holes from the In-X level are recaptured by the deeper indium and divacancy centers. Above 75K, holes begin to be thermally emitted from the indium level. The theoretical model is more fully explained in the Appendix. A similar D_{λ}^* versus temperature curve (Figure 18) was also observed by Rockwell International for a Si:Zn detector (Reference 13). However, the hump in the Si:Zn data is caused by a rise in detector signal, and not by a drop in the noise level. Although the peak at 70K for Si:In was encouraging, in general the D_{λ}^* of this sample was an order of magnitude lower than the detectivity curves of several Si:In samples grown and measured by Hughes Research Laboratories (Reference 14). Because NOSC had difficulty with biasing and measuring the signal of such a large Si:In sample (0.3 cm X 0.5 cm X 0.1 cm), a new set of samples was fabricated with a more preferred configuration of 0.1 cm x 0.1 cm x 0.1 cm.

¹ D_{BB}^* (500K) was converted to D_{λ}^* (6.4 μ m) by multiplying by a factor of 3.

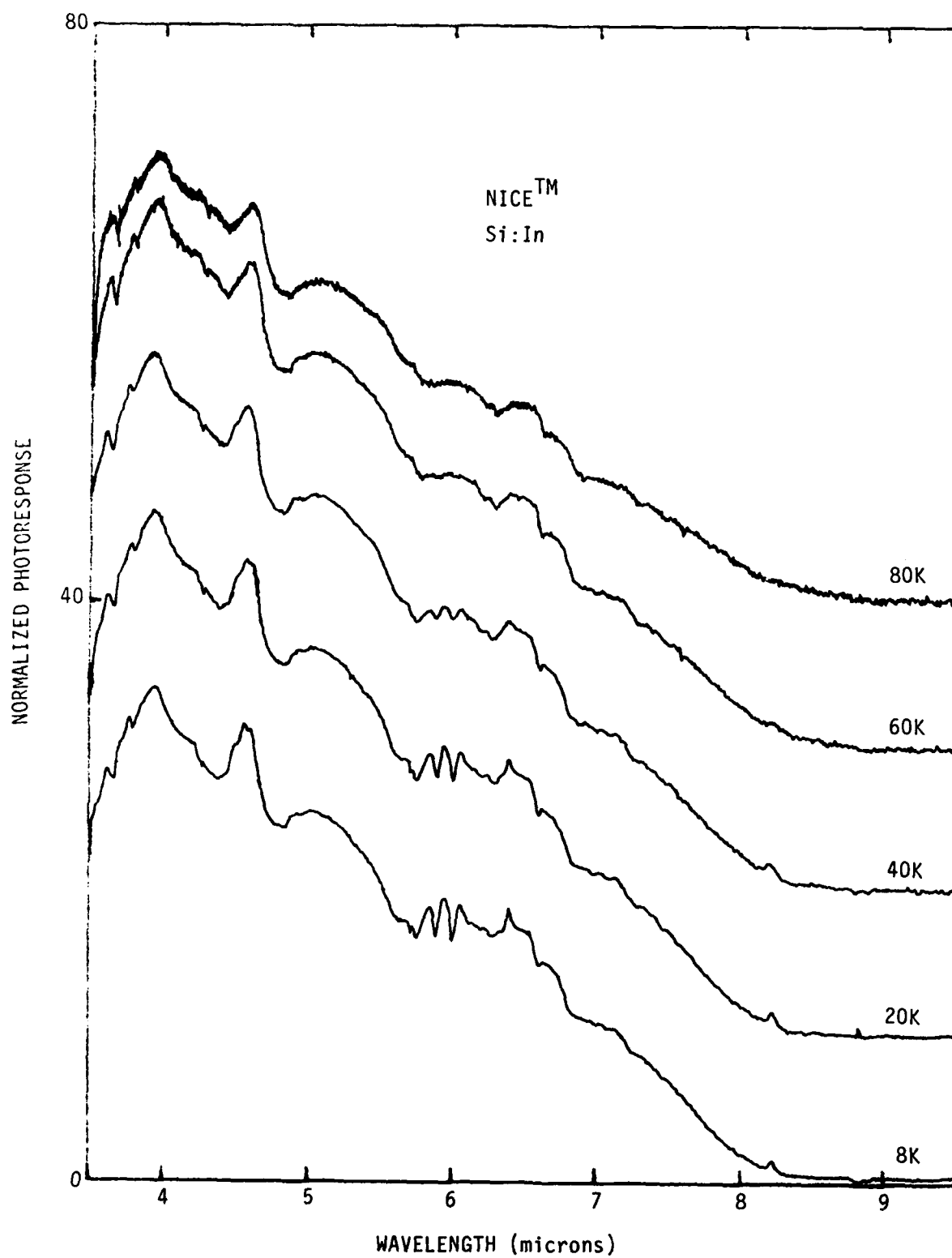


Figure 13. Normalized Photoresponse Versus Wavelength for Electron Irradiated Si:In Sample 0746 from 8K to 80K

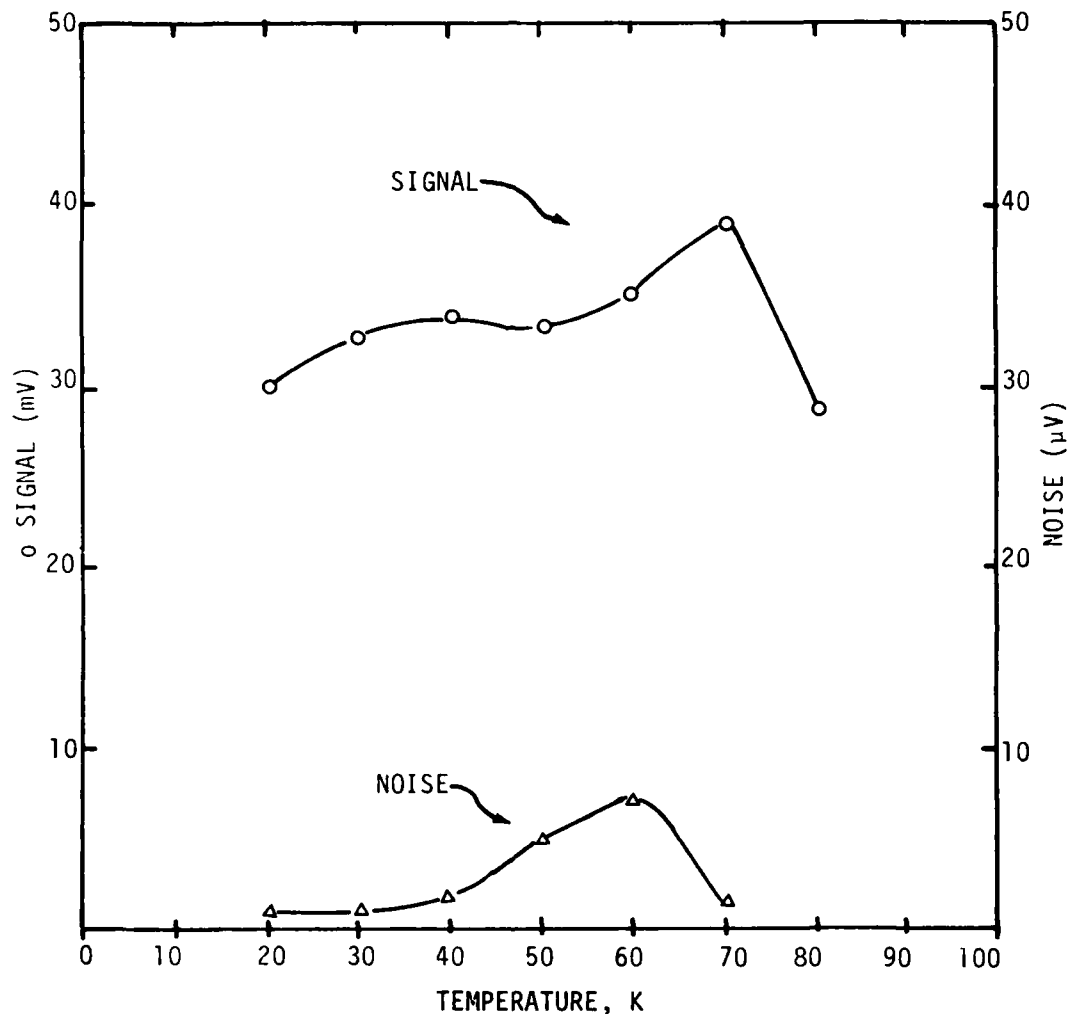


Figure 14. Signal and Noise Levels Measured at 108 hz for Sample 0746

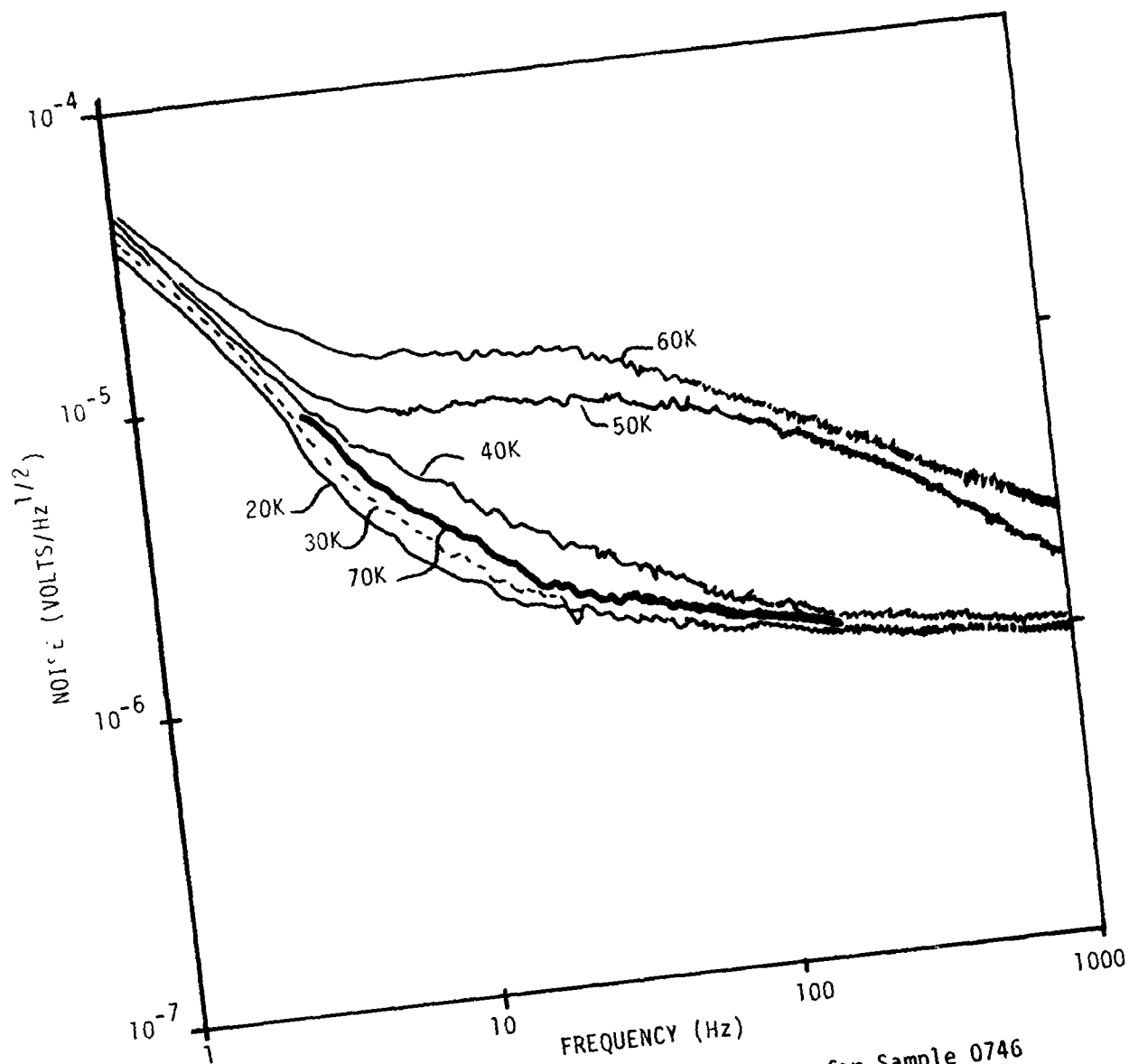


Figure 15. Noise Versus Frequency Data for Sample 0746

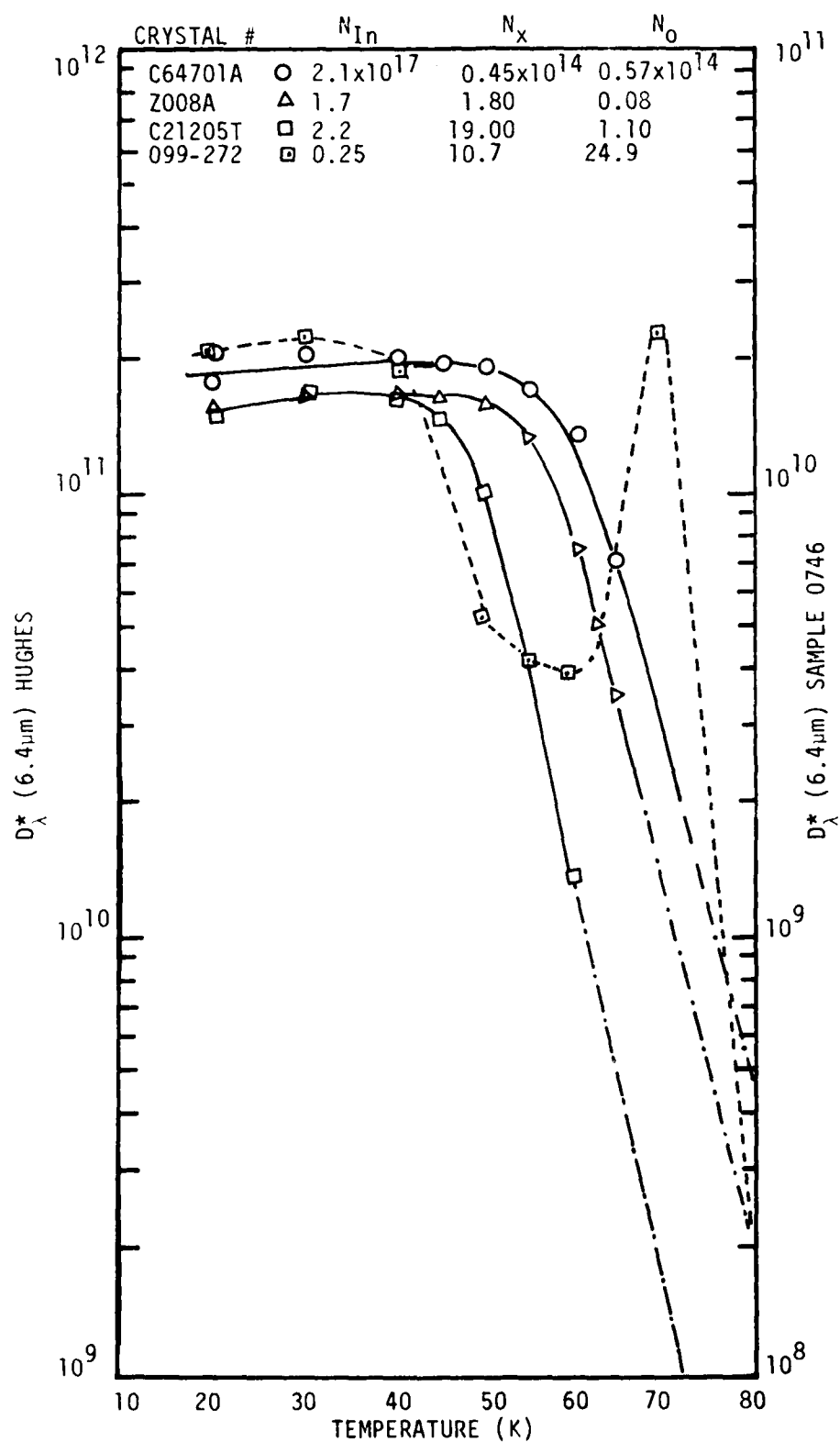


Figure 16. Comparison of D^* Versus Temperature for Sample 0746 and other Detector Grade Si:In Samples

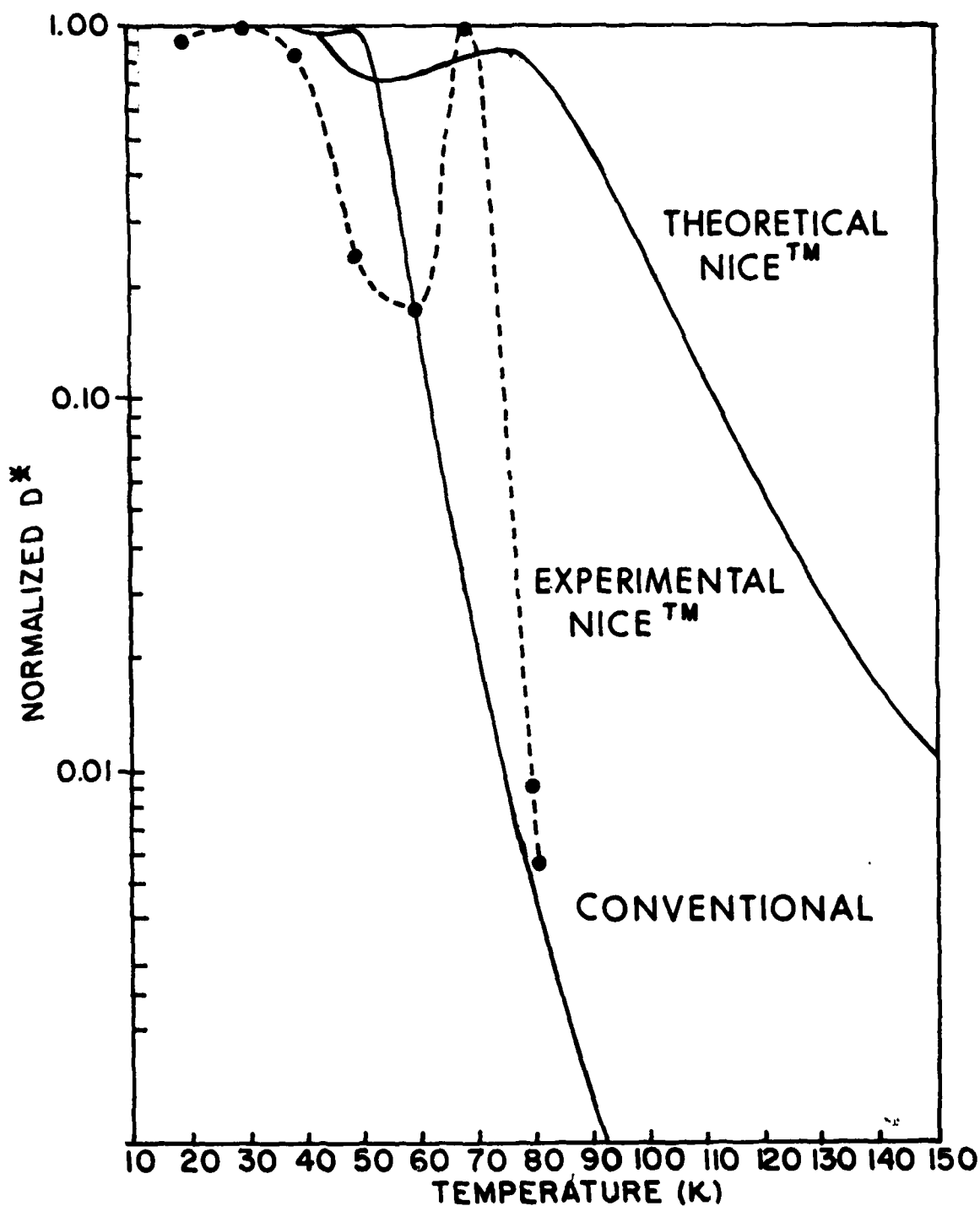


Figure 17. Theoretical Model of Detectivity (D^*) Versus Temperature for a Conventionally Doped Detector and for the Doping Conditions of the NICE™ Detector

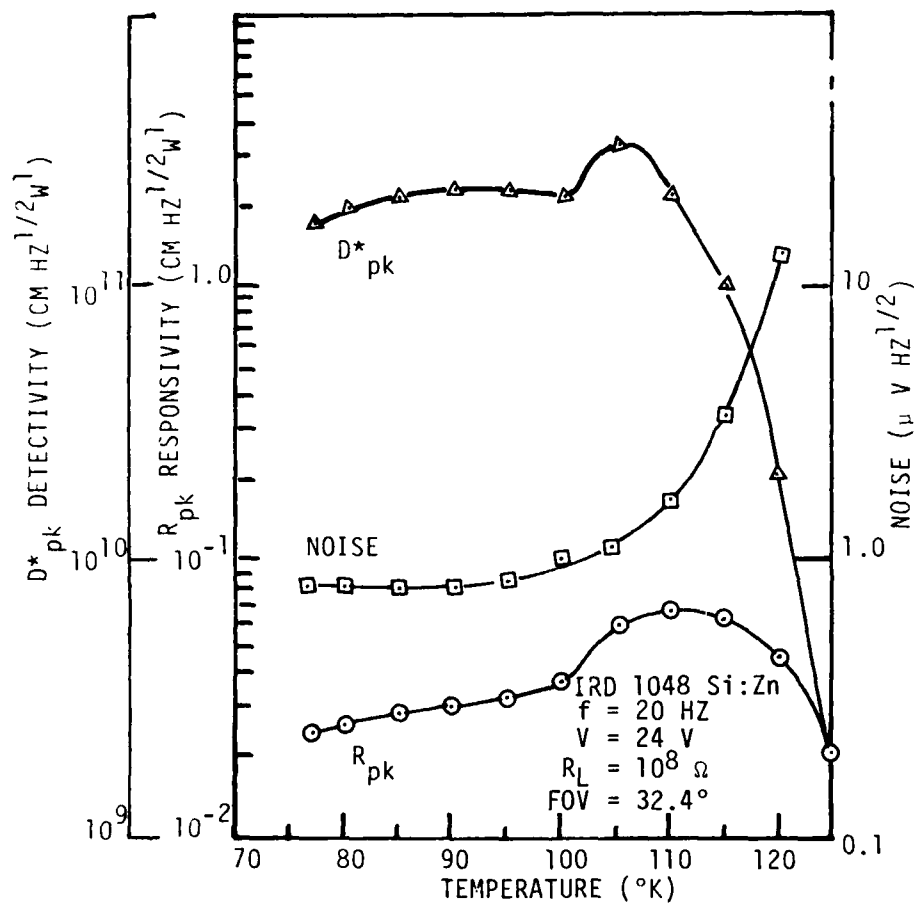


Figure 18. Detector Performance (D^*_{peak}) Versus Temperature for a Diffused Si:Zn Sample

While the new set of samples were being prepared, an as-grown sample from the same wafer was cut for photoconductivity measurements for comparison with the data from the furnace annealed and room temperature annealed electron irradiated samples. A typical spectrum of the as-grown sample (1043) is shown in Figure 19. It was anticipated that the as-grown sample would agree with the 550°C anneal data. Instead sample 1043 had an operating range of 7K to 82K similar to the room temperature annealed electron irradiated (NICETM) sample. However, the rate of increase in the continuum response with temperature was much greater for the as-grown sample than for the NICETM sample. The magnitude and rate of change in response is in agreement with the temperature dependence of the 550°C annealed sample (Figure 20). Still, there is a marked difference in the temperature dependence of these two samples above 20K.

Up to this point it was thought that the electron irradiation had produced the effect that allowed PC data to be collected at temperatures above 30K. There were several papers (References 15, 16, 17) that indicated electron irradiation of doped silicon could produce infrared detectors with higher operating temperatures, up to 100K. In all three papers on electron irradiated Si:B a peak at 4 μ m was observed in the photoionization cross section corresponding to the 0.20 eV divacancy level. The proposed mechanism behind the effect of irradiation on Si:B involved a counterdoped system consisting of the radiation induced divacancy donor level and boron (References 18, 19). Hence, the name New Improved Counterdoped Extrinsic (NICETM) was given for the room temperature annealed, electron irradiated sample. With the unusual temperature dependence of the as-grown sample there came some doubt about whether electron irradiation produced counterdoping was the appropriate explanation for the behavior of the NICETM sample. However, a comparison of the NICETM and the as-grown photoionization cross sections (Figure 21) does reveal a slightly greater response around 4 μ m for the NICETM sample (although weaker than the peak observed in Si:B). At the least the electron irradiation increased the number of donors sufficiently to reduce the boron P_{1/2} band response (Figure 22) as compared to the as-grown sample.

At this time, the new sample set of as-grown and electron irradiated Si:In cubes (0.1 mm x 0.1 mm x 0.1 mm) were ready for photoconductivity measurements. Three cubes of each material were mounted on a beryllium oxide slab to form a mini detector array. Photoconductivity measurements were made on the center cube of each

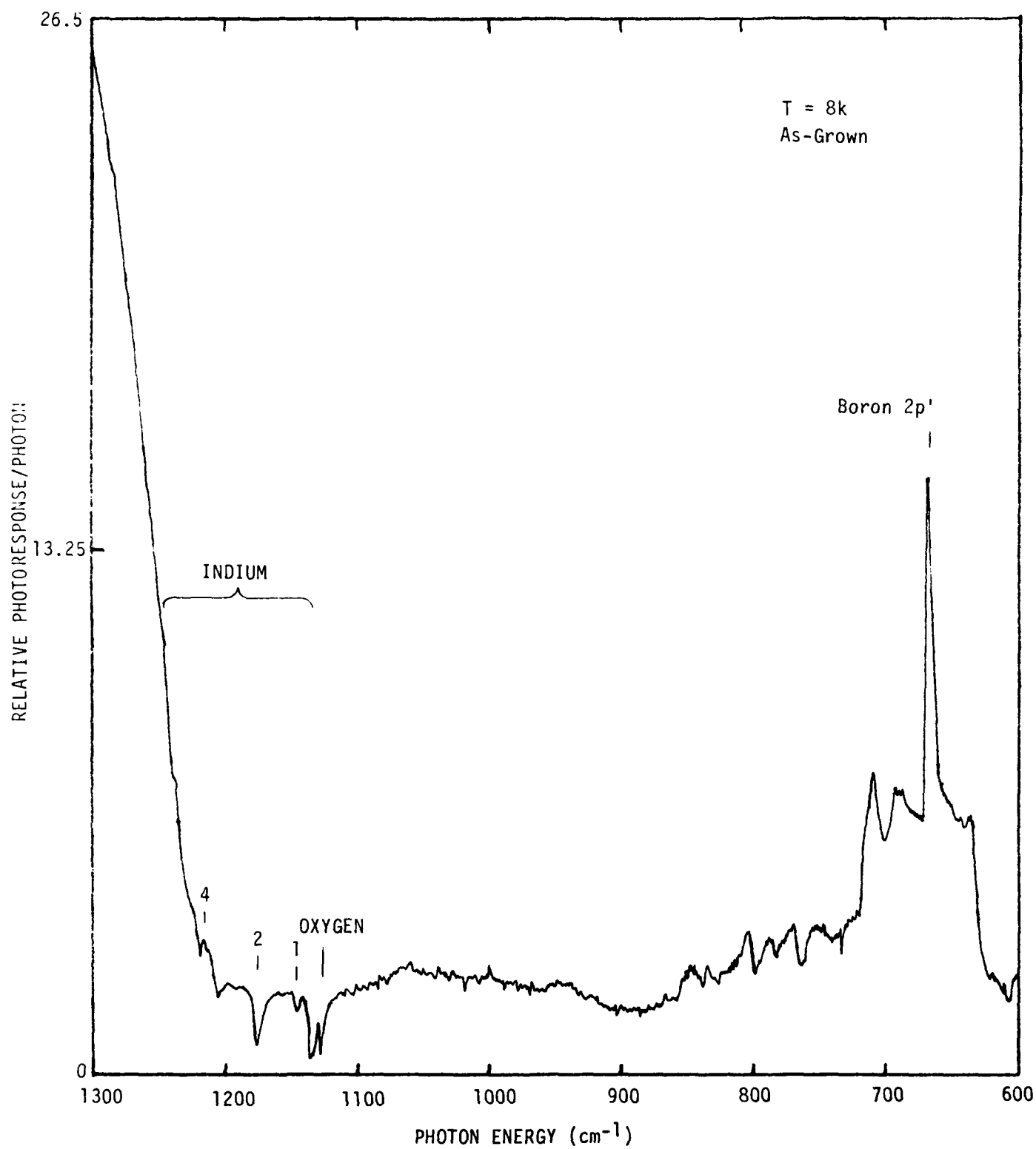


Figure 19. Photoconductivity Spectrum of As-Grown Si:In Sample 1043

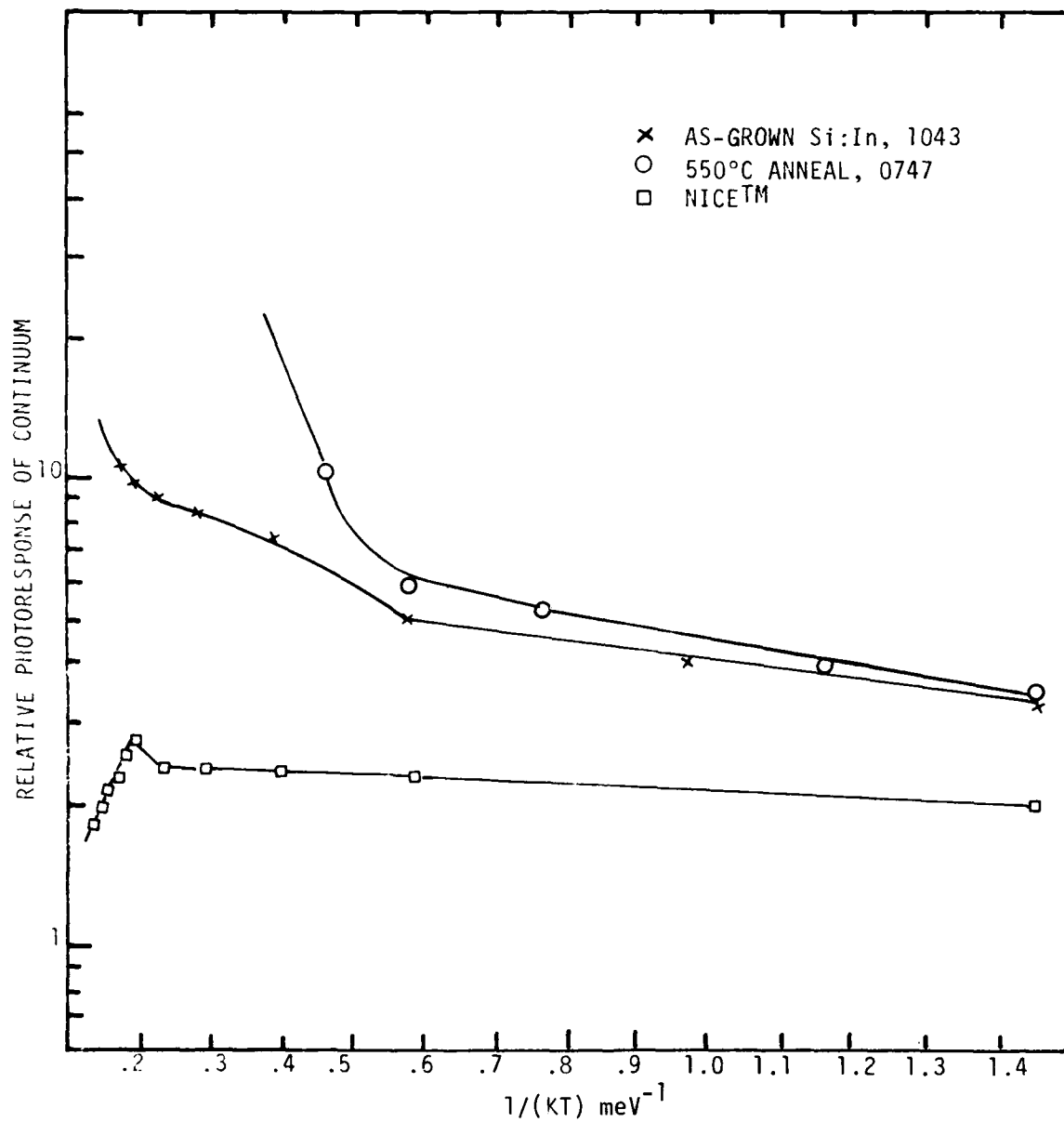


Figure 20. Relative Temperature Dependence of Indium Continuum for As-Grown, Annealed and Electron Irradiated Si:In Samples from Wafer 099-272

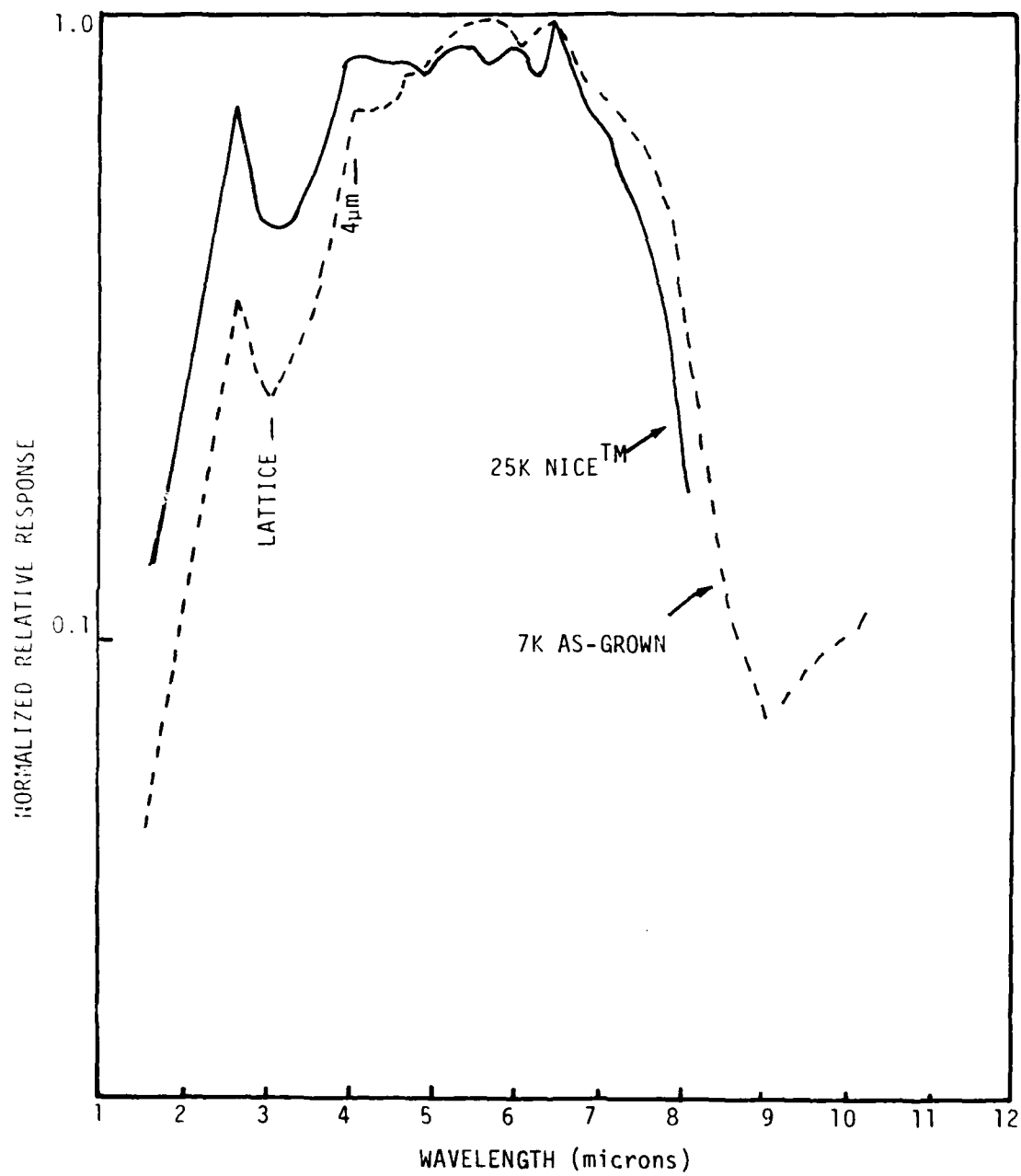


Figure 21. Comparison of the Photoionization Cross Sections of As-Grown and Electron Irradiated Si:In

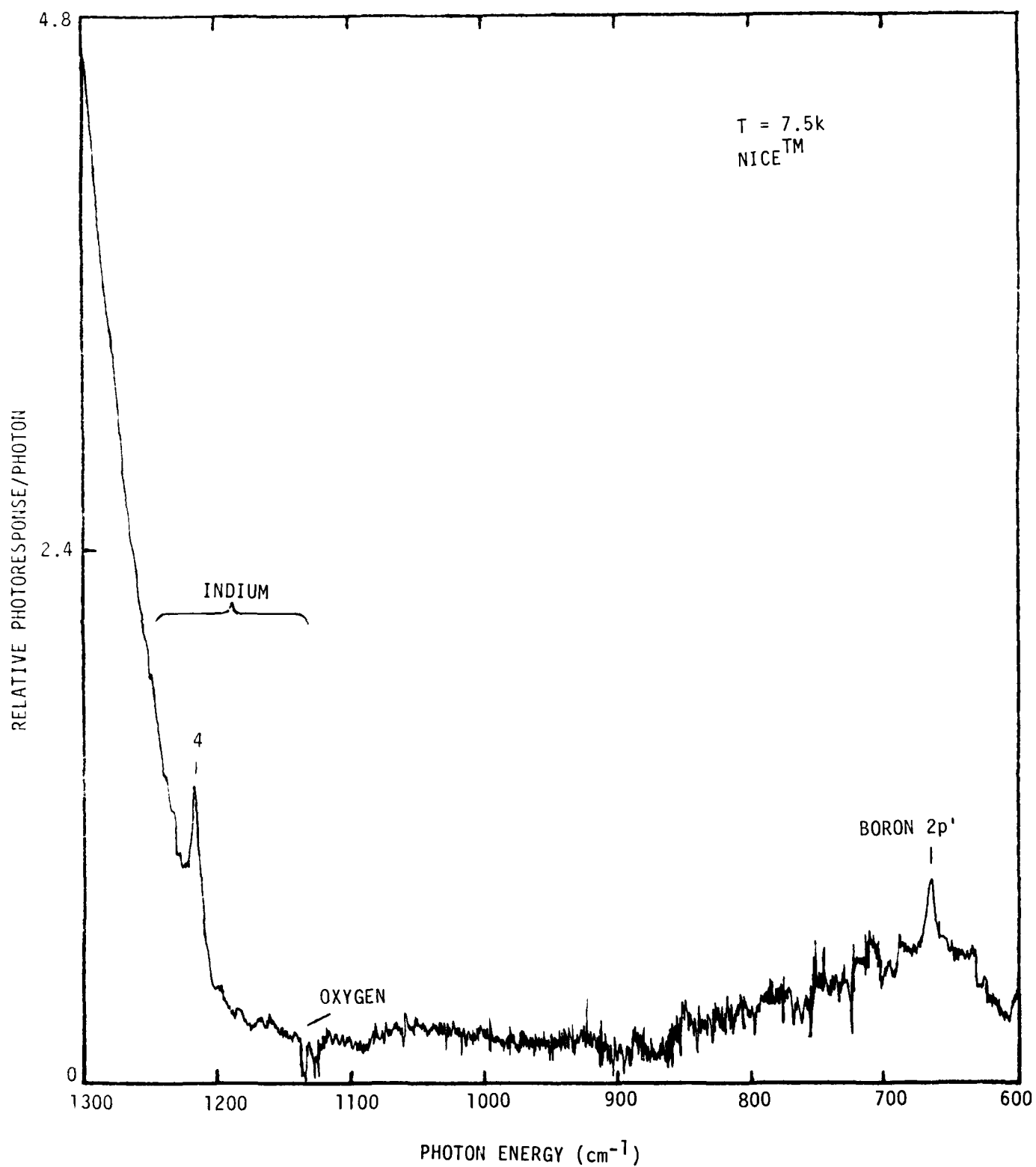


Figure 22. Photoconductivity Spectrum of Electron Irradiated Si:In

array. These measurements agreed well with the previous PC measurements made on the larger samples (0746, 1043). These arrays were then sent to NOSC for infrared detector measurements. Signal and noise measurements were made on the electron irradiated array for 8K to 80K, at bias of 45 volts and a frequency of 108hz (Figure 23). The results of the noise measurements versus frequency are shown in Figure 24. As these curves show, the new set of samples did not exhibit the unusual behavior of the previous NICETM sample at 70K. Using these new measurements the D_{λ}^* versus temperature for NICETM was calculated and graphed in Figure 25. The value of D_{λ}^* , from 8K to 60K, is still an order of magnitude lower than other Si:In infrared detector materials. However, when compared to the results of the as-grown Si:In array, this D_{λ}^* magnitude and operating temperature range is quite remarkable. The as-grown array became extremely noisy above 15K and the detectors broke down at about 22K. Although at 20K the responsivity (amps/watt) of the as-grown detectors was over 400 times greater than that of the electron irradiated detectors, the D_{λ}^* at 20K for the as-grown was only 3.24×10^8 whereas the value for NICETM was 2.27×10^{10} . Clearly the electron irradiation greatly improved the noise level even though it decreased the responsivity somewhat. This decrease in the responsivity is probably caused by the increase in the number of donors after irradiation. As seen previously in the PC data, one large difference between the as-grown and NICETM samples is the size of the boron response. At NOSC there was very little signal beyond eight microns for the NICETM samples. However, the as-grown samples exhibited a large response out to 20 microns. This longer wavelength response is due to the presence of boron, as demonstrated by comparison to our PC measured response (Figure 26). It is this large number of uncompensated boron carriers which causes the as-grown detectors to break down around 20K.

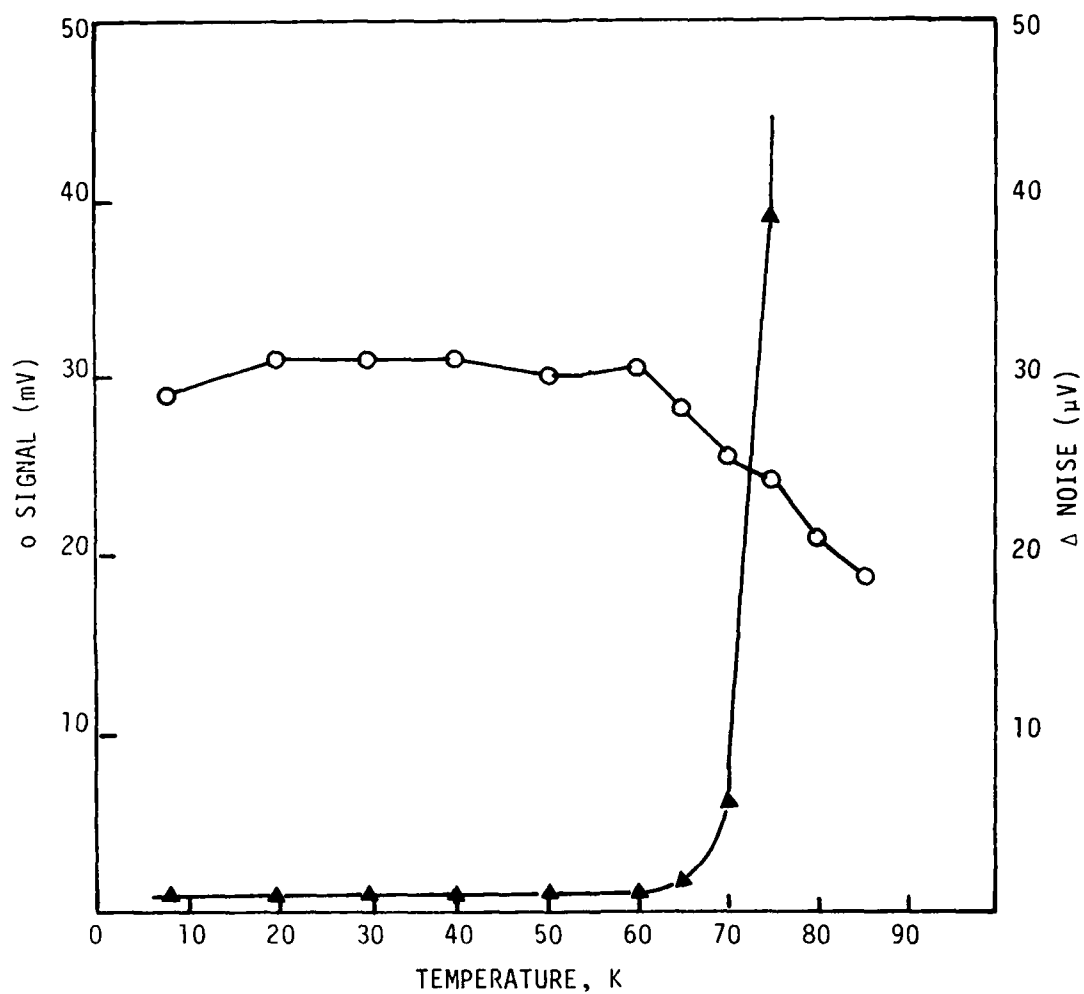


Figure 23. Signal and Noise Levels Measured at 108 Hz for Electron Irradiated Si:In Cubes

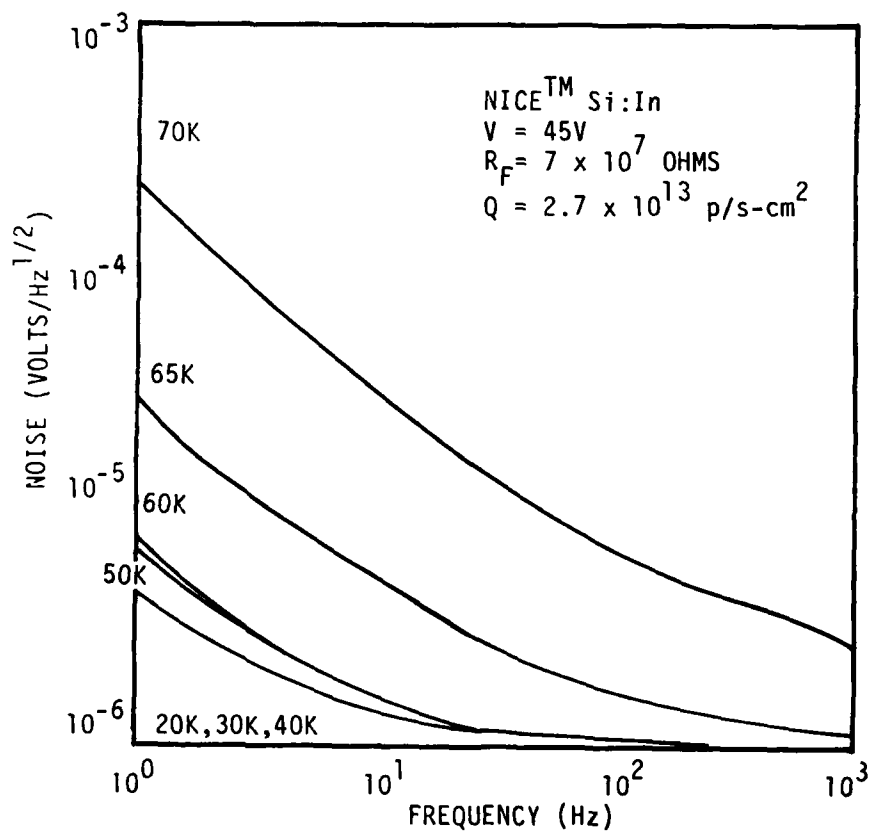
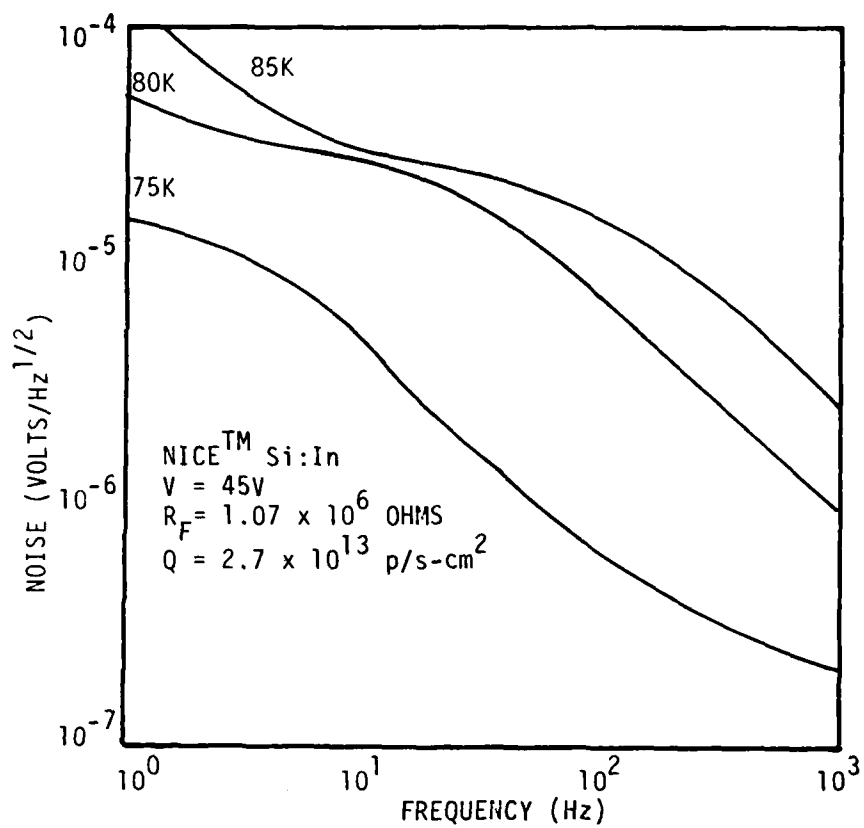
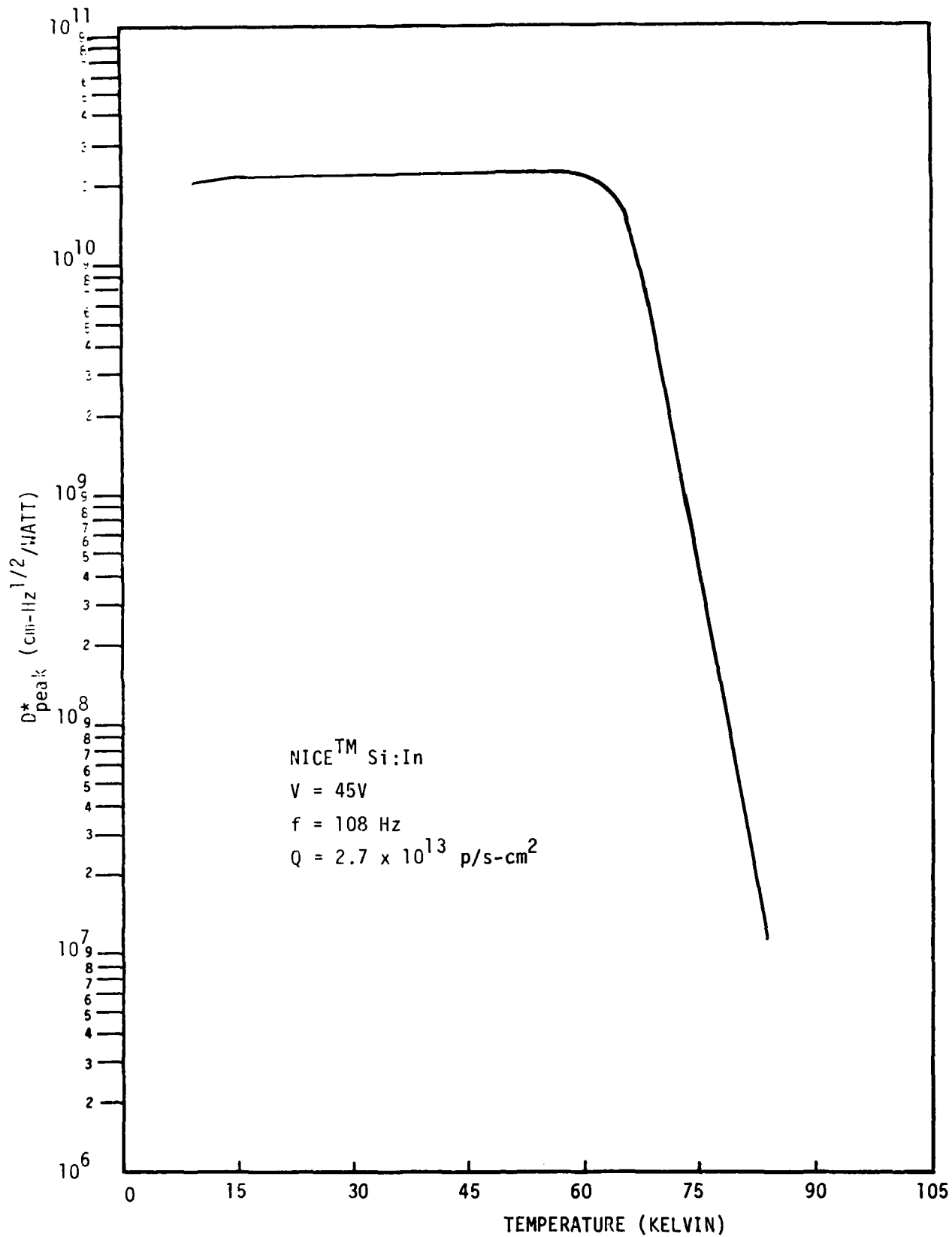


Figure 24. Noise Versus Frequency Data for Electron Irradiated Si:In Cube

Figure 25. Detector Performance (D^*_{peak}) for Electron Irradiated Si:In Cube

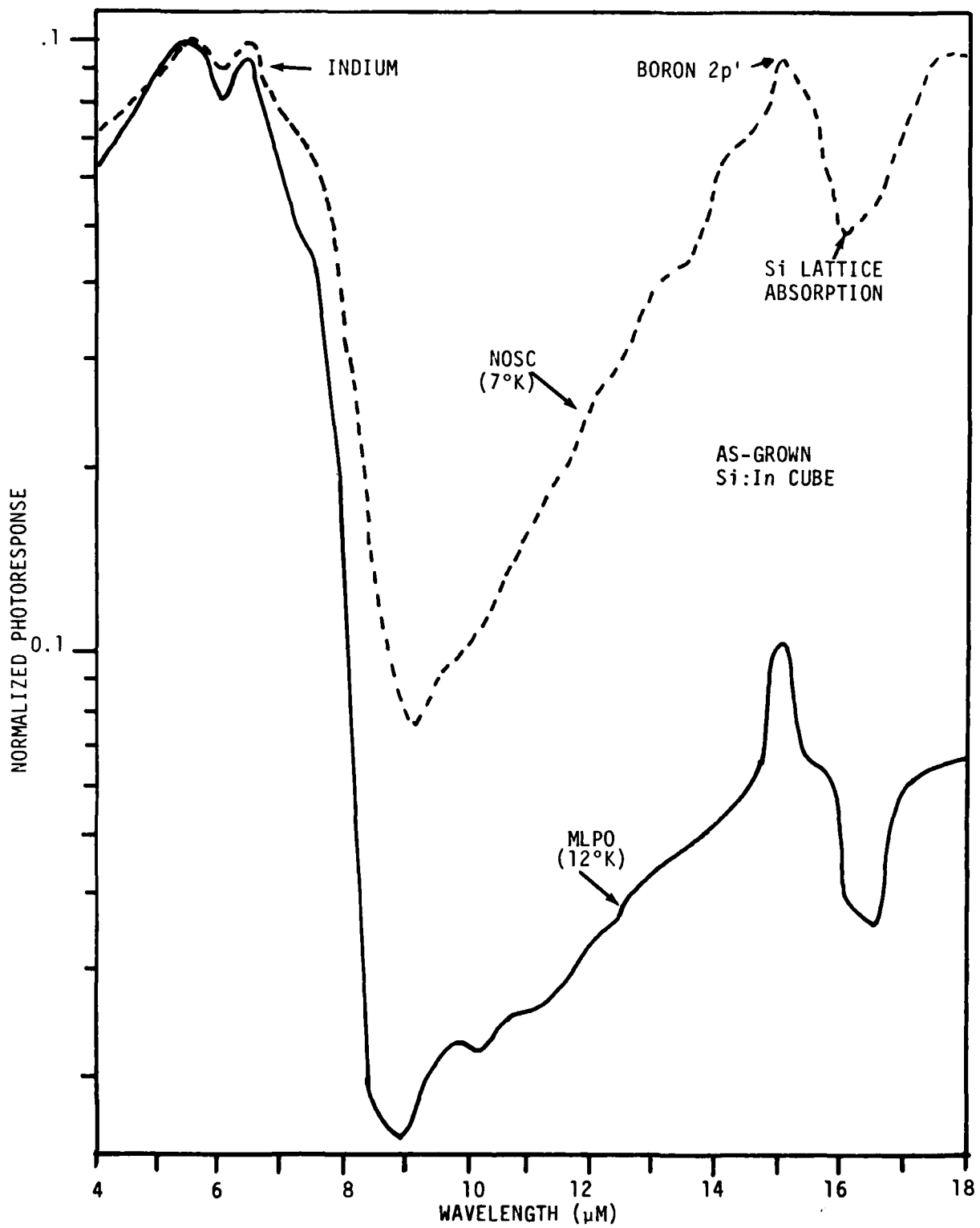


Figure 26. Comparison of NOSC and MLPO Measured Photoresponse of As-Grown Si:In Cube

SECTION IV

CONCLUSIONS AND RECOMMENDATIONS

Based on the NOSC detector measurements and WPAFB photoconductivity data, the electron irradiation of Si:In causes a change in the temperature dependence of the photoresponse and in the level of noise generated by thermal carriers. The mechanism for these changes is not clearly understood. The Hall effect and infrared absorption data detected no unusual behavior for the electron irradiated material. The Hall data "predicts" that the electron irradiated material should have a temperature dependence similar to the as-grown starting material since boron and indium-X are overcompensated in both materials. The infrared absorption data also showed nothing different between the electron irradiated and as-grown materials. Hence, these measurements give no indication of which material parameter was changed by irradiation to improve the detector operating temperature.

However, a comparison of Hall and infrared absorption data does bring up some interesting points. For instance, according to Hall data the indium-X level is no longer overcompensated after the 550°C anneal and should be optically active (Table 4). But the indium-X level is not seen optically after the 550°C anneal. This is probably because the optical cross section of In-X is too small to allow detection of concentrations as low as 2×10^{14} (atoms/cm³). Similarly, boron is overcompensated according to the Hall measurements, and yet boron is seen optically by absorption and photoconductivity (WPAFB and NOSC). Boron is optically active because carriers excited from the indium level are recombining with the compensated boron centers (Reference 20). These comparisons show that the electrical and optical data complement each other in providing information on the active levels in the material.

In addition, the photoconductivity and infrared detector measurements are in good agreement that the electron irradiation of Si:In did increase the operable temperature range of the detector as compared to the as-grown material. In both sets of measurements there was the same flatness of the photoresponse with increasing temperature, up to 65K, for the electron irradiated NICETM samples (Figure 20). Also both sets of measurements on the NICETM samples found the breakdown of the detectors due to thermal noise to occur around 85K. The agreement for the as-grown material measurements was not quite as good. The detector measurements found

TABLE 4
COMPARISON OF IMPURITY CONCENTRATIONS (atoms/cm³) DETERMINED
BY HALL AND INFRARED ABSORPTION MEASUREMENTS

IMPURITY OR DOPANT	HALL		ABSORPTION	
	AS-GROWN	550°C	AS-GROWN	550°C
Indium	1.52×10^{16}	1.98×10^{16}	3.8×10^{16}	3.8×10^{16}
Indium-X	1.92×10^{14}	2.23×10^{14}	---	---
Boron	---	---	no data	2.8×10^{13}
Donors	2.08×10^{14}	1.77×10^{14}	---	---
Carbon	---	---	7×10^{16}	7×10^{16}
Oxygen	---	---	6×10^{17}	6×10^{17}

thermal breakdown to occur around 22K for the as-grown material. The photoconductivity measurements indicated a much higher temperature than 22K. This disagreement over how quickly the noise sets in may be due to the larger boron response measured by NOSC (Figure 26). Overall there is good agreement between the two types of measurements.

The most striking result from the study of electron irradiated Si:In was the detectivity versus temperature data. Though the magnitude of D_{peak}^* was an order of magnitude lower than typical Si:In detector materials, the change in D_{peak}^* with increasing temperature was slightly better than these materials, and a great deal better than our pre-irradiation material. Improving the magnitude of the photoresponse by starting with material with a larger concentration of indium and a lower concentration of donors could make the magnitude of the detectivity more attractive. Unfortunately, there was no Si:In material available with the optimum concentration range to electron irradiate and then check for improvements in the detectivity. However, our non-optimized results do show promise for extending the Si:In detector operating temperature range.

Based on the detectivity measurements for this one wafer of Si:In, it appears that electron irradiation could be a means of creating higher operating temperature extrinsic detectors. To verify this we would recommend several research projects. One project would be to repeat our experiments using a Si:In starting material with a more optimum concentration of dopants, i.e. 2×10^{17} atoms/cm³ of indium and less than 10^{14} atoms/cm³ of boron and donors. Another project would be to electron irradiate a Si:Ga wafer. This would serve two purposes. First, it would check on the advantages of electron irradiation for improving the operating temperature of Si:Ga detectors. And second, since the optical cross section of Si:Ga peaks at 15 μ m, the electron irradiated Si:Ga photoresponse could show a more definite cross section peak at 4 μ m if counterdoping is occurring. Another project would be to experiment with various electron fluences and possible low temperature annealing to optimize the effects of electron irradiation. Overall, the electron irradiation of Si:In has proven to be a fascinating system to study.

APPENDIX

PERFORMANCE MODEL OF A COUNTERDOPED DETECTOR

This appendix deals with the detectivity calculation of indium doped p-type silicon detectors. It is assumed that the concentration of indium is $N_{A1} = 2.5 \times 10^{16} \text{cm}^{-3}$ and that of the In-X centers is $N_{A2} = 1.07 \times 10^{15} \text{cm}^{-3}$. The donor density is $N_D = 2.49 \times 10^{15} \text{cm}^{-3}$. Two parallel calculations will be conducted. In one the donors will be of the usual sort, that is, close to the conduction band edge and totally compensated. The second calculation will be for deep donors such as the divacancies with the energy level 200 meV above the valence band edge.

In either case the detector is taken to be at temperature T and is exposed to the background radiation flux $\phi_B = 10^{13} \text{ photons/cm}^2\text{-sec}$, simulating the experimental conditions for sample 099-272 in the body of the Technical Report. The generation of charge carriers can occur by absorption of a photon, with energy $h\nu$, or by absorption of a quantum of lattice vibration, i.e. phonon with energy $\hbar\omega$. For neutral acceptors the absorption process



produces an ionized acceptor center and a positively charged hole in the valence band. For positively charged donors the absorption process



results in a neutral donor and a hole in the valence band. The valence band holes can be swept out by the applied field and constitute the current. There is also an inverse process by which the holes recombine with the centers. The two processes are



neutralizing the acceptor, and



which compensates the donor. Both Equations A3 and A4 are accompanied by liberation of energy, most likely in the form of phonon emission. It is assumed that Equations A3 and A4 are the primary lifetime-limiting mechanisms operative in the detector.

In order to calculate the detector figure-of-merit figures one must solve the rate equations appropriate to the detector. The rate at which neutral acceptors, either In or In-X, are produced is given by

$$\frac{\partial N_A^0}{\partial t} = p B_A N_A^- - N_A^0 \langle \sigma_A \phi \rangle - N_A^0 \frac{B_A}{g_A} N_V e^{\frac{E_V - E_A}{kT}}, \quad (A5)$$

where

- g_A = Degeneracy of the acceptor level
- B_A = The recombination coefficient for the process Equation A3
taken to be $6 \times 10^{-4} / T^{1.5} \frac{\text{cm}^3}{\text{sec}}$.
- p = Hole concentration
- N_A, N_A^0, N_A^- = Total acceptor, neutral acceptor, and ionized acceptor concentrations
- σ_A = The peak photoabsorption cross section for the acceptors, taken to be $1.8 \times 10^{-15} \text{cm}^2$.
- ϕ = Photon flux (photons/cm²-sec)
- N_V = Effective density of states in the valence band
- E_A = Ionization energy of the acceptor level, 156 meV for In and 112 meV for In-X.

For each acceptor level

$$N_A = N_A^0 + N_A^-, \quad (A6)$$

so that in the steady-state

$$N_A^- = \frac{\alpha_A N_A}{p + \alpha_A} \quad , \quad (A7)$$

where

$$\alpha_A = \frac{N_V}{g_A} e^{\frac{E_V - E_A}{kT}} + \frac{\langle \sigma_A \phi \rangle}{B_A} \quad . \quad (A8)$$

Similarly we can write the rate equation for the formation of ionized donor centers as

$$\frac{\partial N_D^+}{\partial t} = B_D p N_D^0 - g_D B_D N_V e^{\frac{E_V - E_D}{kT}} N_D^+ - N_D^+ \langle \sigma_D \phi \rangle \quad , \quad (A9)$$

where the physical constants have the same meaning as in Equation A5 but in relation to the donor level. We take $g_D=2$, $\sigma_D=5.4 \times 10^{-16} \text{ cm}^2$, and $B_D=6 \times 10^{-10}/T^{1.5} \text{ cm}^3 \text{ sec}^{-1}$ for sake of concreteness. Note that B_D is million times smaller than B_A since the hole capture rate by neutral centers, process (Equation A4), is much less likely than the capture by negatively charged centers, process (Equation A3). In steady state

$$N_D^+ = \frac{N_D p}{\alpha_D + p} \quad (A10)$$

where

$$\alpha_D = N_V g_D e^{\frac{E_V - E_D}{kT}} + \frac{\langle \sigma_D \phi \rangle}{B_D} \quad . \quad (A11)$$

If the donor level is near the conduction band then the exponential in Equation A11 is practically zero and the absorption cross section is zero at infrared wavelengths. Therefore, for simple donors, like phosphorus

$$N_D^+ = N_D \quad . \quad (A12)$$

For divacancies with $E_D - E_V = 200$ meV this is not necessarily so and the donors play an active role in the charge balance equation.

The charge balance equation

$$N_{A_1}^- + N_{A_2}^- = P + N_D^+ \quad (A13)$$

with Equation A7 for N_A^- and Equation A10 for N_D^+ gives rise to the quartic equation for p :

$$\begin{aligned} p^4 + p^3 (\alpha_{A_1} + \alpha_{A_2} + \alpha_D + N_D) \\ + p^2 [\alpha_{A_1} \alpha_{A_2} + \alpha_{A_1} \alpha_D + \alpha_{A_2} \alpha_D + \alpha_{A_1} (N_D - N_{A_1}) + \alpha_{A_2} (N_D - N_{A_2})] \\ + p [\alpha_{A_1} \alpha_{A_2} (N_D + \alpha_D) - \alpha_{A_1} N_{A_1} (\alpha_{A_2} + \alpha_D) - \alpha_{A_2} N_{A_2} (\alpha_{A_1} + \alpha_D)] \\ - \alpha_{A_1} \alpha_{A_2} \alpha_D (N_{A_1} + N_{A_2}) = 0 \end{aligned} \quad (A14)$$

If $N_D = N_D^+$ for the conventionally compensated detector, then Equation A13 gives rise to the cubic equation for p :

$$\begin{aligned} p^3 + p^2 (N_D + \alpha_{A_1} + \alpha_{A_2}) + p [\alpha_{A_1} \alpha_{A_2} - \alpha_{A_1} (N_{A_1} - N_D) - \alpha_{A_2} (N_{A_2} - N_D)] \\ + \alpha_{A_1} \alpha_{A_2} (N_D - N_{A_1} - N_{A_2}) = 0 \end{aligned} \quad (A15)$$

The different forms of Equations A14 and A15 are the result of the fact that the donor in Equation A14 actively exchanges holes with the valence band while in Equation A15 the donors are mere "spectators" of the processes involving acceptors only.

Equations A14 and A15 can be solved for p given the doping conditions, temperature, and the background flux. The figures of merit for the two types of detectors are calculated using the methods explained in detail by McGuigan, Szmulowicz, and Hemenger (Reference 21). The responsivity is shown to be

$$R \sim \left(\frac{\partial p}{\partial \phi} \right)_{\phi_B}, \quad (A16)$$

and the detectivity is proportional to

$$D^* \sim \left(\frac{1}{p} \frac{\partial p}{\partial \phi} \right)^{\frac{1}{2}}. \quad (A17)$$

The detectivity of the conventionally compensated system and of the NICETM detector were shown in Figure 17. At low temperatures (without the background flux on) the donor electrons compensate the shallowest acceptors. With the background flux on, electrons from the valence band are promoted to the deeper indium acceptor levels and to the divacancy levels in the case of the deep donor. This results in largely neutral In-X, compensated In, and largely neutral divacancy levels. At low temperatures (before thermal ionization of In-X) the main noise mechanism in the detector is the background radiation induced generation-recombination noise. The detector is then background limited resulting in a flat, temperature independent detectivity versus temperature plot.

As temperature increases, holes are thermally emitted by In-X which increases the thermal contribution to the generation-recombination noise. In the conventional doping scheme some of these holes are recaptured by the negatively charged indium centers. This has the effect of repairing the detectivity slightly which explains the slight shoulder at about 50K in Figure 17 for the conventional detector. Subsequently, indium itself is thermally depopulated which leads to the sharp thermal rolloff above 50K.

In the deep donor counterdoping scheme both the ionized indium and the neutral donors act as effective hole sinks for the holes thermally emitted by the In-X levels. Therefore, above 50K this type of the detector should tend back toward the background limited behavior since In-X becomes exhausted of holes which now reside on much deeper centers as the temperature is increased beyond 75-80K range in Figure 17. Since many holes have been captured at the relatively deep donor level the thermal rolloff due to indium is delayed toward higher temperatures where the donor level becomes saturated with holes captured from the valence band, i.e. $N_D \approx N_D^+$. At this temperature the thermal rolloff becomes evident.

Figure 17 displays a high temperature peak similar to that measured for the NICETM detector. The model described in this Appendix relies on many parameters which may or may not have been realized in the NICETM sample. The least known numbers are the recombination coefficients B. Choices of these parameters were reasonable orders of magnitude estimates. To within liberal variations of

these parameters the qualitative behavior of D^* in Figure 17 is still valid. In particular, it is σ/B which has to be reasonably estimated rather than σ or B alone (see Equations A8 and A11).

In conclusion, the model described herein simulates the experimental conditions as we know them and produces the detectivity curve similar to that measured for the NICETM detector. Further experimental data is necessary to verify assumptions in the model for a more positive correlation between experiment and theory.

REFERENCES

1. V. Swaminathan, J. E. Lang, P. M. Hemenger, and S. R. Smith, Appl. Phys. Lett., 35, 184 (1979).
2. S. R. Smith and R. Harris, Proc. IRIS Special Group Meeting on IR Detectors (1981), F8, Sep., 1982, p. 445.
3. L. J. van der Pauw, Philips Res. Rpts., 13 1, (1958).
4. J. A. Amick, Solid State Technology, Nov 1976, p. 47.
5. B. C. Dobbs, P. M. Hemenger, and S. R. Smith, J. Electron, Mater., 6, 705, (1977).
6. K. R. Bradley and P. M. Hemenger, Bull. APS, 26, 5, (1981).
7. P. M. Hemenger, Rev. Sci. Instrum., 44, 698, (1973).
8. F. L. Madarasz, J. E. Lang, and P. M. Hemenger, J. Appl. Phys., 52, 4646, (1981).
9. J. E. Lang, F. L. Mararasz, and P. M. Hemenger, J. Appl. Phys., 54, 3612, (1983).
10. J. E. Lang, Private communication
The functional form used for the Hall scattering factor as a function of temperature was:

$$r(T) = 0.54 + \frac{1.22}{1.0 + (T/50)^2}$$
11. D. K. Schroder, T. T. Braggins, and H. M. Hobgood, J. Appl. Phys., 49, 5256, (1978).
12. J. I. Pankove, Optical Processes in Semiconductors, Dover Publications, Inc., 1971.
13. N. Sclar, Materials for MOSIS FLIR (Monolithic Silicon Sensor FLIR), Final Report for ANVL Contract (DAAG 53-76-C-0208), p. 4-20.
14. R. Baron, M. H. Young, J. P. Baukus, O. J. Marsh, and M. J. Sheets, Proc. of the IRIS Specialty Group on Infrared Detectors, 1977 (Infrared Information and Analysis Center, Ann Arbor, Michigan, 1977), Vol. I.
15. C. Gross, R. J. Mattauch, and T. J. Viola Jr., J. App. Phys., 44, 735 (1973).
16. E. F. Maher, D. V. Eddolls, B. R. Holeman, and R. G. Humphreys, Electronics Lett., 18, 216 (1982).
17. S. D. Brotherton, G. J. Parker, and A. Gill, J. Appl. Phys., 54, 5112 (1983).
18. C. T. Elliot, P. Migliorato, and A. W. Vere, Infrared Phys., 18, 65 (1978).

REFERENCES (Concluded)

19. E. F. Maher and D. V. Eddolls, Workshop on Silicon for Infrared Applications, Univ. of Erlangen, Oct., 1981.
20. D. W. Fischer, J. Appl. Phys., 56, 2984 (1984).
21. J. McGuigan, F. Szmulowicz, and P. M. Hemenger, A Model of the Performance Characteristics of Silicon-Gallium Infrared Detectors for Low Background Applications, AFWAL-TR-84-4035, Materials Laboratory, Air Force Wright Aeronautical Laboratories, Wright-Patterson Air Force Base, Ohio 45433-6533, April 1984.

END

FILMED

4-8

DTIC